Modeling of cationic lipid-DNA complexes

S. May[a] **and** ⋆**A. Ben-Shaul**[b]

[a]Institut für Molekularbiologie, Friedrich-Schiller-Universität Jena,
Winzerlaer Str. 10, Jena 07745, Germany
Tel: 49-3641-657582, Fax: 49-3641-657520, email may@lily.molebio.uni-jena.de

[b]Department of Physical Chemistry and the Fritz Haber Research Center,
The Hebrew University, Jerusalem 91904, Israel
Tel: 972-2-6585271, Fax: 972-2-6513742, email abs@fh.huji.ac.il

Abstract

Cationic lipid–DNA complexes, often referred to as *lipoplexes*, are formed spontaneously in aqueous solutions upon mixing DNA and liposomes composed of cationic and nonionic lipids. Understanding the mechanisms underlying lipoplex formation, structure and phase behavior is crucial for their further development and design as non-viral transfection vectors in gene therapy. From a physical point of view, lipoplexes are ordered, self-assembled, composite aggregates. Their preferred spatial geometry and phase behavior are governed by a delicate coupling between the electrostatic interactions which drive lipoplex formation and the elastic properties of the constituent lipid layers, both depending on the molecular nature and composition of the lipid mixture. In this review we outline some recent efforts to model the microscopic structure, energetics and phase behavior of cationic lipid-DNA mixtures, focusing on the two principal aggregation geometries: the lamellar (L_α^C), or "sandwich" complexes, and the hexagonal (H_{II}^C), or "honeycomb" complexes. We relate the structural and thermodynamic properties of these two "canonical" lipoplex morphologies to their appearance in phase diagrams of DNA-lipid mixtures, emphasizing the crucial role fulfilled by the molecular packing characteristics of the cationic and neutral lipids, as reflected in the curvature elastic properties of the mixed lipid layer.

key words: Lipoplex, Electrostatics, Membranes, Curvature Elasticity, Phase Transitions, Lamellar and Hexagonal Phases, Isoelectricity

List of abbreviations:

CL: cationic lipid

DOPE: dioleoylphosphatidylethanolamine

DOSPA: 2,3-dioleyloxy-N- [2(sperminecarboxamido)ethyl]-N,N-dimethyl-1-propanaminium trifluoroacetate

ds: double stranded

PC: phosphatidylcholine

DOTAP 1,2-dioleoyl-3-(trimethyammonium) propane

PE: phosphatidylethanolamine

PB: Poisson-Boltzmann

1 Introduction

Adding DNA to an aqueous solution containing liposomes composed of cationic and electrically neutral ("helper" or "co-") lipids, results in the disruption of part or all of the liposomes and the spontaneous appearance of composite cationic lipid-DNA (CL-DNA) structures, or *lipoplexes*. The formation of CL-DNA complexes is driven by The formation of CL-DNA complexes is driven by the strong electrostatic attraction between the cationic lipid headgroups and the negatively charged phosphate groups on the DNA backbone. This attraction, as will be further discussed in later sections, is mediated by the release of the small mobile ("counter") ions into solution upon DNA-lipid complexation, and the concomitant gain in their translational entropy. This gain is maximal at the "isoelectric point" when the total lipid charge exactly balances the total DNA charge. This notion, and the strong electrostatic driving force for complex formation imply that either all the cationic lipids, or all the DNA, or both are complexed. That is, when a small amount of lipids is mixed with excess DNA, all lipids become involved in complex formation whereas part of the DNA remains "naked" in solution. In the opposite limit, corresponding to excess lipid in solution, only a fraction of the liposomes is involved in complexation of all the DNA. Though not carrying electric charges, because of their ability to tune both the surface charge density and the curvature elastic properties of the mixed lipid layers, the helper lipids play a crucial role in determining the optimal aggregation geometry of CL-DNA complexes.

Our primary goal in this review is to highlight the principles governing the interplay between electrostatic lipid-DNA interactions and lipid elasticity, the dependence of this coupling on the nature and composition of the lipid layers and lipid-DNA ratio, and the reflection of these factors in the morphological, energetic and thermodynamic characteristics of lipoplex phase behavior. Most of the concepts to be discussed are of direct relevance to a variety of other membrane-macromolecule interactions, e.g., protein adsorption onto biomembranes. The following sections of this review will focus on the theoretical-physical concepts underlying lipoplex structure and phase behavior. It is therefore appropriate to begin the discussion with a brief survey of the experimental background and biomedical relevance of these systems. Further details can be found in other chapters of this volume.

Lipoplexes are currently the most promising non-viral gene delivery vehicles into mammalian cells. Among the advantages of these transfection vectors, as compared to their viral counterparts, are their negligible immunogenicity response, and the ease of their large scale production [1, 2]. In fact, as already noted above, formation of lipoplexes requires barely more than mixing DNA with liposomes, in strong contrast to the elaborate gene splicing protocols in viral gene therapy. On the other hand, controlling the size and shape of the complexes is rather intricate and requires detailed understanding of the kinetic and thermodynamic mechanisms underlying complex formation. Furthermore, the transfection efficiency of lipoplexes is generally much lower than that of viral vectors. The design of improved transfection vectors has thus become the major challenge in non-viral gene delivery, initiating the synthesis of numerous different cationic lipids and their subsequent testing in lipoplex formulations and transfection experiments. In parallel, much effort has been devoted to investigating the relation between lipoplex structure and transfection efficiency [3, 4, 5]. Thus far, many details of lipoplex-induced transfection remain unresolved. This concerns all steps from lipoplex assembly, targeting, internalization into the cell, disassembly and the ultimate translocation into the cell nucleus [6, 7].

The necessary steps for successful delivery of nucleic acids require a number of different, sometimes conflicting, properties of the lipoplexes. For example, larger amounts of cationic lipids facilitate binding to the cell surface but also increase cytotoxicity [8]. Moreover, the lipoplexes must be stable enough to survive the journey towards and across the plasma membrane into the cell interior. Yet, once inside the cell, these complexes should be "fragile" enough in order to decompose and release their DNA content into the cytoplasm [9]. Clearly then, understanding the factors governing the energetic, structural, and thermodynamic

characteristics of CL-DNA complexes is essential for optimizing their transfection efficiency [10].

Most phospholipids in aqueous solution self-assemble into *planar bilayers*, often closing upon themselves to form vesicles. Other phospholipids, such as dioleoylphosphatidylethanolamine (DOPE), because of their relatively small headgroup, prefer the packing geometry of the *inverse-hexagonal* (H_{II}) phase [11]. The lipid layers composing these structures are "soft", self-assembled, aggregates. On the other hand, double stranded (ds) DNA, which serves as the genetic material in most lipoplexes, is a rigid rod-like molecule showing negligible structural flexibility. The structure of the CL-DNA complexes emerging in solution is thus dictated by the molecular packing propensities of their constituent lipids, which can rearrange their packing geometry upon complexation with DNA. The resulting lipoplex geometry reflects the balance between the packing propensities of the lipid molecules and electrostatic interactions with the DNA rods.

In some of the earliest studies of lipid-DNA complexation it was assumed that the liposomes remained intact (or perhaps reorganized into lipid micelles), with the DNA binding to their surface [12, 13]. Somewhat later, electron microscopy studies clearly indicated drastic reorganization of the liposomes and complete encapsulation of the DNA by the lipids [14, 15]. These experiments revealed a rich polymorphism of CL-DNA aggregates, and provided approximate information about their size and shape. Based on their visual appearance some of the observed structures were given rather pictorial names such as "beads on a string" [13], "spaghetties" or "meatballs" [16, 17], inspiring the use of terms like "honeycomb" and "sandwich" complexes for other structures in subsequent studies.

It did not take long before molecular-level structural information had been reported based on X-ray studies, indicating that lipoplexes are periodic structure of both the (rod-like) double stranded DNA (dsDNA) rods and the lipid layers constituting the composite complexes [18, 19, 20, 21, 22, 23]. In particular, the X-ray measurements revealed the existence of two "canonical" packing orders: *lamellar* and *hexagonal* [18, 19], identical to the symmetries of the lamellar (L_α) and hexagonal (H_{II}) liquid crystalline phases of pure lipid assemblies. The observed ordered CL-DNA complexes have thus been termed "L_α^C" and "H_{II}^C" phases. It is now known that lipoplex structure and stability depend on many factors, including the molecular characteristics of the cationic and helper co-lipids [24, 25], the chemical composition of the lipid mixture, the length and type of the DNA (e.g., circular versus linear), and the ambient conditions such as pH, salt concentration and temperature [19, 26, 27].

Fig. (**1**) shows three basic geometries of CL-DNA complexes. The L_α^C, or "sandwich" complex (A) is a lamellar stack of cationic-nonionic lipid bilayers, intercalating monolayers of parallel dsDNA rods. (The term "rod" is fully justified here in view of the fact that the persistence length of dsDNA, $\xi \approx 500$ Å, is much larger than its 20 Å diameter. It is also much larger than the thickness of the lipid bilayers or the intervening water gaps, both on the order of 30 Å.) The DNA rods within a given gallery are equally spaced, with a uni-dimensional (1D) correlation length extending over about ten DNA molecules, as evidenced from the line shape analysis of x-ray scattering data [28, 29]. The distance, d, between adjacent dsDNA's in a given gallery depends on the composition of the lipid layers, typically in the range $25\,\text{Å} \leq d \leq 70\,\text{Å}$, with d decreasing as the mole fraction of the cationic lipid increases [18]. Noting that the radius of dsDNA is $R_D \approx 10$ Å, it follows that the minimal spacing between adjacent rods, $d \approx 25$ Å, corresponds to nearly close DNA-DNA contact, with only a thin hydration shell separating between adjacent DNA strands. The thickness of the water gap between adjacent lipid bilayers is similar, $w \approx 26$ Å, corresponding again to near contact between the DNA rods and the lipid layers, with thin water shells between their surfaces. However, unlike d which varies with the lipid composition, w is nearly constant in all lamellar complexes. The freedom to adjust the DNA-to-DNA spacing is a unique property of the L_α^C complex. It adds to the ability of these complexes to optimize their lipid composition in the presence of excess lipid in solution. The origin of these phenomena will be discussed in the following sections.

In the H_{II}^C, or "honeycomb" [30], complex shown in Fig. (**1B**) dsDNA rods are intercalated within the aqueous tubes of an hexagonal lipid matrix. The symmetry of this structure is identical to that of the

inverse-hexagonal, H_{II}, phase of (DNA free) lipids [11]. Owing to the stringent constraints on the lipid chain packing in the H_{II} phase, the diameter of the water tubes in this array, for most lipids of biological interest, are typically just a few Å's larger than the diameter of dsDNA. In other words, the DNA rods can comfortably be accommodated within the hollow water tubes of the hexagonal lipid array. Strong electrostatic attractions between the phosphate charges on the DNA surface and the surrounding cationic headgroups tend to minimize the distance between the lipid and DNA surfaces, setting it to one or two water molecule diameters. The spacing of the hexagonal DNA array is thus fixed, corresponding to roughly twice the thickness of the (mixed) lipid monolayer. This, in turn, implies a specific given number of lipid molecules per unit length of DNA in the H_{II}^C complex. Thus, the only degree of freedom left for the H_{II}^C complex is the lipid composition. We shall see below how the different degrees of freedom of the L_α^C and H_{II}^C complexes are manifested in the phase diagrams of CL-DNA mixtures.

Another complexation geometry, which unlike the lamellar and hexagonal structures, does not exhibit long range order, is the "spaghetti"-like complex illustrated in Fig. (**1C**) [31]. This structure, which has been suggested based on electron microscopy studies, consists of (supercoiled) DNA surrounded by a cationic lipid bilayer. As these structures often appear to emerge from more compact aggregates or are connected to semi-fused liposomes, one may speculate that the "spaghetti" complexes are transient structures, possibly serving as precursors to the H_{II}^C phase. This notion is supported by theoretical calculations revealing that the

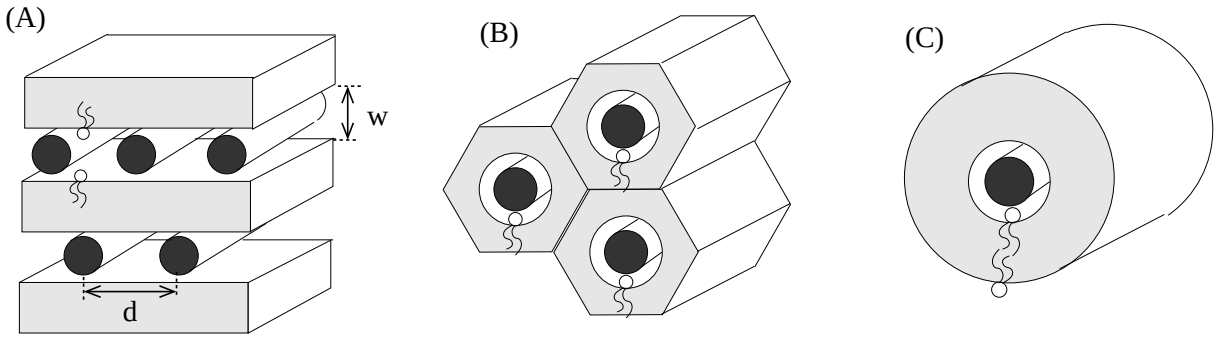

Figure 1: Illustration of three principal lipoplex geometries: The lamellar (L_α^C) or "sandwich" structure (A), the hexagonal (H_{II}^C) or "honeycomb" complex (B), and the bilayer-coated, or "spaghetti", complex (C). The light-shaded areas represent the hydrophobic cores composed of lipid hydrocarbon chains, a few of which are schematically drawn. The solid circles indicate DNA cross-sections. In (A), *w* is the thickness of the water gap between adjacent lipid bilayers, and *d* is the DNA-DNA distance.

spaghetti complex is a metastable structure, of higher free energy than that of the corresponding H_{II}^C complex [30]. The H_{II}^C phase, as seen in Fig. (**1B**), can be viewed as an hexagonal array of dsDNA's, wrapped around by lipid monolayers. Similarly, the spaghetti complex consists of the same central structural element, i.e., a monolayer-coated DNA, which instead of being associated with identical elements (as in H_{II}^C complexes) is wrapped around by another (oppositely bent) lipid monolayer.

Biomedical studies suggest that the transfection efficiency of lipoplexes is correlated (though in a non-trivial way) with the propensity of their constituent lipids to assemble into curved, non-bilayer, structures [32]. To a large extent, the optimal curvature of the lipid mixture is dictated by the type and concentration of nonionic co-lipids in the complexes, which, in turn (and, again, in a nontrivial way) depends on the initial composition of the liposomal lipid reservoir. Another important role of the neutral lipids is in tuning the cationic charge density on the lipidic surface. The simultaneous tuning of both the charge density and the curvature of the lipid layers plays a principal role in determining the preferred geometry, the stability and

the lipid composition of the lipoplex.

The repeat distance of base pairs along the axis of dsDNA is 3.4 Å, implying (on average) a 1D density of one phosphate charge per $l = 1.7$ Å along the DNA axis. Assuming that the phosphate charges are uniformly spread over the surface of a cylinder of radius $R_D = 10$Å corresponding to the (hard core) radius of dsDNA, we find that the charge density on the DNA surface is $\sigma_D = -e/2\pi l R_D = -e/110\,\text{Å}^2$. The charge density of the cationic lipid layer, $\sigma_B = e\phi/a_h$, depends on the mole fraction of the cationic lipid, ϕ, and the cross-sectional area per lipid, as measured at the headgroup surface where the cationic charge resides. Earlier in this section it was noted that maximal complex stability is achieved at the *isoelectric point* where the magnitudes of the total DNA and lipid charges are equal. For planar membranes, such as those in the lamellar lipoplex, charge matching is obtained when $\sigma_D + \sigma_B = 0$. The cross-sectional area per lipid headgroup is typically $a_h \approx 70\text{Å}^2$, leading to charge matching for $\phi = 0.65$. The optimal lipid composition corresponding to the hexagonal complex is quite different, and depends on the radius R_L of the cylindrical envelope containing the cationic headgroups. For close contact, at $R_L = R_D + 3$ Å, the matching composition is $\phi = 0.35$ [33].

Recent modeling [34, 35] and experimental studies [36] suggest that isoelectricity alone may not suffice to explain all the structural characteristics of lipoplexes. These studies indicate a direct involvement of the neutral, zwitterionic, phosphatidylcholine (PC) lipids in the electrostatic interaction with the DNA: The P^-–N^+ dipole of PC headgroups is well known to be almost parallel to the bilayer plane [37]. Yet, in mixtures with cationic lipids the anionic phosphate of PC interacts preferentially with the charge of the co-lipid, resulting in reorientation of the P^-–N^+ dipole towards the aqueous environment [38] and a corresponding decrease in the cross-sectional area of PC [39]. It is thus the N^+ end of the P^-–N^+ dipole of the PC co-lipid that interacts most favorably with the complexed DNA. Whether similar mechanisms apply in systems involving other co-lipids remains to be established.

The equilibrium geometry of a self-assembled aggregate composed of two or more lipid species reflects the packing characteristics of the individual lipid components. Thus a large fraction of "curvature loving" lipids in the mixture will generally result in the formation of curved aggregates. Note that the preferred (or "spontaneous") curvature of the lipids may either be 'positive', as in micellar aggregates, or 'negative', as in the H_{II} phase. Generally, we refer to positive (negative) curvature of a lipid layer for bending towards (away from) the hydrocarbon core, as is schematically illustrated in Fig. 2. Cone-shaped phospholipids, such as the single-chain lysolipids are characterized by a relatively large headgroup area, a_h, and small cross-sectional tail area, and thus self-assemble into spherical or cylindrical micelles. Yet, a_h is not necessarily determined by the steric size of a headgroup; it is also affected, often dominated, by the strength of inter headgroup interactions, primarily electrostatic and hydration forces. Indeed, the double-tailed multi-cationic lipid 2,3-dioleyloxy-N- [2(sperminecarboxamido)ethyl]-N,N-dimethyl-1-propanaminium trifluoroacetate (DOSPA) shows a pronounced tendency to form micellar aggregates [40]. On the other hand, double chain lipids with small headgroups tend to form inverted micellar structures, in which the lipids adopt (on average) the shape of an "inverted cone". This is typically the case for lipids with a phosphatidylethanolamine headgroup (PE's). The relatively small cross-sectional area a_h results from a strong intermolecular hydrogen bond network that prevents the formation of a large hydration shell. Notably, dioleoylphosphatidylethanolamine (DOPE), which is an often used co-lipid, shows a pronounced tendency to form the inverse-hexagonal (H_{II}) phase. Most double-chained lipids are characterized by comparable cross-sectional areas of the headgroup and tail regions, and their molecular shape is roughly that of a "cylinder", intermediate between a "cone" and "inverted cone". These lipids, including PC and various charged lipids, self-assemble into planar bilayers. Similarly, most (monovalently charged) cationic lipids, like the often used 1,2-dioleoyl-3-(trimethyammonium) propane (DOTAP), tend to assemble into planar bilayers. When a cationic lipid species is mixed with DOPE (or a similar H_{II} phase-forming lipid) the mixed system undergoes a structural transition from the H_{II} to the L_α phase as the mole fraction ϕ of the cationic lipid increases.

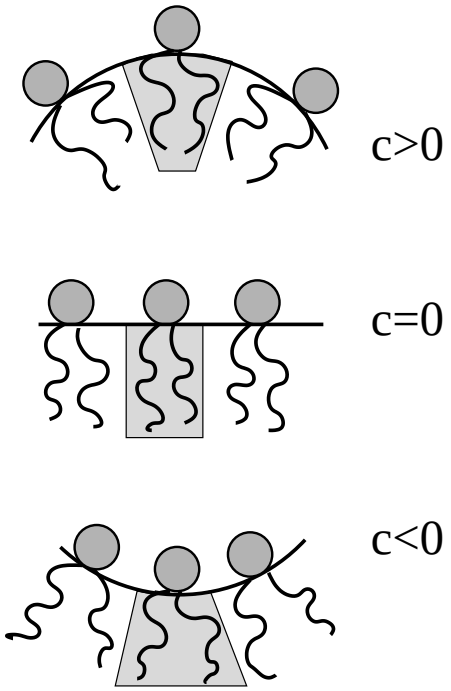

Figure 2: Schematic illustration of lipid layers with positive ($c > 0$), vanishing ($c = 0$), and negative ($c > 0$) curvature. Cone-shaped lipids such as the single-chain lysolipids tend to self assemble into positively curved lipid layers. Inverted cone-shaped lipids such as DOPE prefer negative curvature. Most double-chained and monovalently charged (including cationic) lipids tend to adopt planar membranes where $c = 0$.

In addition to their potential use in non-viral gene therapy, lipoplexes are composite "super-structured" assemblies with remarkable thermodynamic properties that pose a number of theoretical challenges. Combined with the growing need to correlate lipoplex structure and transfection efficiency, they have inspired quite a few theoretical studies, particularly (though not exclusively [30]) following the structural determination of the lamellar complex [18]. Modeling studies have addressed both microscopic and macroscopic length scales; with methods ranging from atomic-level computer simulations [34] to liquid crystal elasticity theory [41]. Most theoretical treatments employ mean field approaches and focus on the crucial role of electrostatic interactions between DNA and cationic membranes; see e.g., [30, 42, 43, 44, 45, 46, 47, 48] and the review in [49].

The focus of our theoretical discussion below is on the interplay between elastic and electrostatic interactions governing lipoplex formation, and their role in determining the thermodynamic phase behavior of lipid-DNA mixtures. Rather than starting from the microscopic-structural level and then gradually evolving through mesoscopic-structural issues towards the thermodynamic phase behavior, we have chosen to follow the opposite direction. That is, examining one "generic" phase diagram of a lipid-DNA solution, we shall first qualitatively analyze its gross features and the gradually unfold its microscopic origin. We open the discussion, in Sec. 2, with the presentation and preliminary analysis of a rather complicated, yet not atypically complicated, phase diagram, calculated for a lipid mixture involving a curvature-loving helper lipid. In Sec. 3 we introduce the free energy contributions to lipoplex formation, emphasizing the electrostatic, elastic and lipid mixing terms, and analyze their coupled role in two important phase transitions that appear as special cases in the calculated phase diagram: The L_α-H_{II} transition in pure lipid assemblies (Sec. 3), and the L_α^C-H_{II}^C transition describing the morphological transformation between lamellar and hexagonal CL-

DNA complexes (Sec. 4). Equipped with the necessary theoretical tools, we separately analyze in Sec. 5 the structure and energetics of the L_α^C and H_{II}^C complexes. Sec. 6 is devoted to one particular aspect of the L_α^C phase, namely, bilayer curvature modulations and their role in correlating between DNA monolayers in different galleries. Finally, Sec. 7 returns to the calculated phase diagram and discusses the role of the co-lipid. We finish with a short summary of our major conclusions in Sec. 8.

2 Phase behavior

Fig. (**3**) displays a calculated, generic, phase diagram of system containing dsDNA and curvature-loving lipid mixture. More specifically, the two-component lipid mixture consists of a cationic lipid (DOTAP, for example) preferring the packing environment of a planar bilayer, and a curvature-loving helper lipid (e.g., DOPE) which, alone in solution, self-assembles into H_{II} aggregates. Qualitatively, this rather formidable theoretical phase diagram [33] accounts faithfully for the rich and complex phase behaviors exhibited by similar lipid-DNA mixtures. It is consistent with experimental studies pertaining to specific regions in the diagram [19, 40], as outlined below.

Two levels of theoretical modeling are necessary in order to derive (and analyze) such phase diagrams. First we need the formation free energies of the different possible phases, as a function of their compositional and structural degrees of freedom. Five phases are relevant here: the naked dsDNA (*D* in the phase diagram); two (DNA free) binary lipid phases, namely, the planar bilayer, L_α phase (*B*, for "bilayer" in the diagram), and the inverse-hexagonal H_{II} phase (*I* ="inverse"); and, of course, the two lipoplex phases, i.e., the lamellar-sandwich L_α^C (*S*="sandwich" in the diagram) complex, and the hexagonal-honeycomb H_{II}^C lipoplex (*H*="honeycomb"). Evaluating the formation free energies of these phases requires molecular level modeling of the electrostatic, elastic and compositional degrees of freedom, as detailed in the following sections.

The second stage in deriving the phase diagram involves the solution of the thermodynamic equations governing the multitude of possible phase equilibria in the system. These are the conditions for the equality of the chemical potential of each species (cationic lipid, co-lipid and DNA) in all coexisting phases. Thermodynamically, these conditions express the requirement for minimal free energy of the entire DNA-lipid mixture with respect to all relevant degrees of freedom, i.e., the relative proportions of the different possible phases, their lipid composition and their internal structure (e.g., d in the case of the sandwich complexes). Actually, the phase diagram in Fig. (**3**) was calculated by direct numerical minimization of the total free energy [33]. The five possible structures were treated as macroscopic phases, thereby ignoring all the surface (finite-size) effects, which can be important (yet highly specific and generally unpredictable) in the case the lipoplexes are small.

The phase diagram in Fig. (**3**) is presented in terms of the two most significant, experimentally controllable, composition variables. One of these is the overall lipid composition of the system, ϕ, measuring the mole fraction of CL in the lipid mixture. The other is the ratio, ρ, between the total numbers of positive (cationic) and negative (DNA) charges in solution. Equivalently, ρ is the ratio between the number of (monovalent) cationic lipids and DNA phosphate groups. When $\rho = 1$ the system is isoelectric.

For given temperature, salt content and pH, the two intensive variables ρ and ϕ provide a full thermodynamic description of the system phase behavior. It should be noted that the aqueous solution embedding the five (condensed) phases in Fig. (**3**) does not play a direct role in affecting the phase behavior of the system (except for serving as a heat and mobile ion reservoir). In other words, there are only three relevant chemical components in the system: DNA and the two lipid species. At a given temperature and pressure the system may be mono-, bi- or even tri-phasic. The plethora of coexistence regimes in Fig. (**3**), including several three phase equilibria, indicates that for certain ϕ, ρ combinations only small free energy differences distinguish between several possible phases.

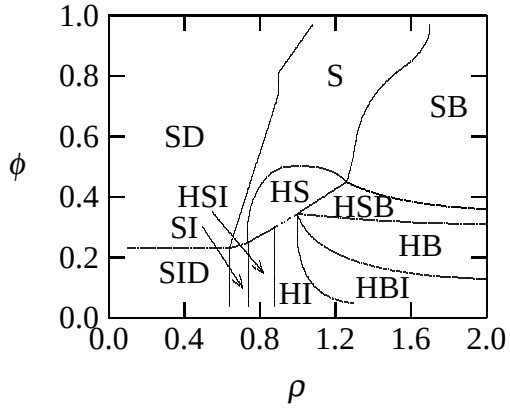

Figure 3: Generic phase diagram of a lipid-DNA mixture containing a "curvature-loving" co-lipid and bilayer-loving cationic lipid, calculated as a function of the mole fraction of the cationic lipid, ϕ, and the lipid-to-DNA charge ratio ρ. The symbols *S*, *H*, *B*, *I* and *D* denote, respectively, the L_α^C, H_{II}^C, L_α, H_{II}, and uncomplexed (naked) DNA phases. The diagram involves one phase regions, e.g., in the region labeled *S* all DNA and lipids are associated to form sandwich-like (L_α^C) lipoplexes. Similarly, *SD*, for instance, is a biphasic coexistence region of sandwich lipoplexes and naked DNA, and *HSI* is a region of three phase equilibrium involving honeycomb and sandwich complexes as well as a binary inverse-hexagonal lipid phase. The short dashed line marks the single H_{II}^C phase (from Ref. [33], with permission).

Using a lipid mixture composed of a curvature-loving co-lipid (e.g., DOPE) and a bilayer forming cationic lipid (e.g., DOTAP), one expects the appearance in solution of either lamellar (L_α^C or *S*), or hexagonal (H_{II}^C or *H*) lipoplexes, or both, depending of course on ρ and ϕ. Indeed, the phase diagram in Fig. (**3**) exhibits both the H_{II}^C and L_α^C structures, appearing either as single phases, or in various two- and three-phase coexistence regions.

Despite its complicated appearance the principal qualitative predictions of the phase diagram in Fig. (**3**) are not too difficult to understand. Let us briefly summarize the major conclusions. The inverse-hexagonal lipid packing – appearing in both the H_{II} and H_{II}^C structures – dominates in the regions of small ϕ, where the lipid mixture involves a large fraction of the curvature-loving helper lipid. Similarly, the phases involving planar lipid bilayers – the L_α and L_α^C structures – dominate the high ϕ, CL rich, regions. Most regions in the phase diagram involve uncomplexed phases: naked DNA (*D*) for small ρ, where the amount of lipid in solution does not suffice to complex all the DNA, and pure lipid phases (*B* and/or *H*) at high lipid contents.

Complete association of the lipid and DNA molecules is limited to a rather narrow portion of the phase diagram, centered around the isoelectric line $\rho = 1$. We note a monophasic region of (nearly isoelectric) lamellar lipoplexes (*S*), when the lipid mixture is rich in the bilayer-forming cationic lipid component. Both types of lipoplexes coexist within the narrow region (*HS*) of the phase diagram. A single phase of hexagonal complexes is possible only within a minute regime of the phase diagram, corresponding to the short dashed line in Fig. (**3**).

Varying the lipid composition along a path from $\phi = 1$ to $\phi = 0$ at constant ρ, amounts to diluting the cationic charge in the lipid layers by a gradual increase of the helper lipid mole fraction. Ultimately, this process must lead to the appearance of an excess lipid phase, even for $\rho = 1$. However, the existence of a finite (albeit narrow) monophasic regime where $\rho \neq 1$ indicates that the ability of a lipoplex to deviate

from isoelectricity and tolerate a certain excess of either positive or negative charge. This, "overcharging" capability, is a general property of interacting macroions in aqueous solution [49]. When used for transfection, lipoplexes are commonly prepared to be positively overcharged in order to facilitate their interaction with the negatively charged plasma membrane; subsequent internalization of the lipoplexes is believed to proceed via endocytosis [50].

Experimental observations are consistent with the phase diagram in Fig. (**3**). For example, the L_α^C-H_{II}^C transition was originally observed by Koltover et al [19] upon dilution with curvature-loving co-lipids at the isoelectric point ($\rho = 1$). In another experimental study, Simberg et al [40] have analyzed the phase behavior of a DOTAP/DNA mixture for different values of ρ and found good agreement with the predictions of Fig. (**3**). Note also that the ability of a CL-DNA mixture to adopt the H_{II}^C complex structure appears often correlated with transfection efficiency [51], and is possibly caused by the destabilization of (endosomal) bilayers upon contact with non-lamellar phase-preferring co-lipids [52].

Simpler phase behavior is expected, for instance, when both lipid species show strong preference for the planar bilayer geometry, in which case the lipoplexes are likely to be lamellar in most, possibly all, regions of the phase diagram. While reasonable, this qualitative argument is not invariably valid, because strong electrostatic forces may compete, possibly suppress, the elastic propensities, resulting for instance in the formation of hexagonal complexes even when both lipids prefer the planar bilayer geometry. In the next section we consider this balance of forces in more detail, focusing on the morphological phase transition between the lamellar and inverse-hexagonal phases in (DNA-free) lipid mixtures, thus preparing the ground for the analogous, yet more intricate transition between lamellar and hexagonal lipid-DNA lipoplexes, to be discussed in Sec. 4.

3 The L_α-H_{II} transition of cationic lipid mixtures

Upon incorporating curvature loving helper lipids such as DOPE into a lipid bilayer, a morphological transformation from the planar to the inverse-hexagonal symmetry ($L_\alpha \to H_{II}$) sets in at a certain, sharply defined, bilayer composition. The lipid composition of the inverse-hexagonal phase is generally different from that of the bilayer, naturally richer in the curvature-loving lipid. The separation of the lipid mixture into two coexisting phases of different compositions resembles similar phase equilibria in mixed systems, e.g., binary liquid solutions, yet an important difference must be noted: while phase separation in liquid or solid solutions are generally driven by the nonideal mixing of the two components, the lamellar-to-hexagonal transition takes place even if, within each phase, the two components are ideally mixed. The transition is driven, of course, by the different packing propensities of the two components: one tending to organize into planar bilayers while the other into inversely curved layers; as illustrated in Fig. (**4**). The transition sets in when the "frustration" energy involved in packing the two lipid components in one, uniformly mixed, phase becomes intolerable, resulting in a first order *morphological-compositional* phase separation. In this section we discuss the free energy contributions responsible for this transition, setting the background for the analogous, but more complex, $L_\alpha^C \leftrightarrow H_{II}^C$, transition in lipoplex solutions.

The L_α and H_{II} phases are condensed lipid mixtures, embedded in an aqueous solution. The solution's characteristics such as temperature and mobile ion concentrations enter the thermodynamic analysis only indirectly, through their influence on electrostatic and other inter-lipid interactions. What we need then for modeling the $L_\alpha \leftrightarrow H_{II}$ transition is the free energy of the lipid mixture, possibly partitioned into these two phases, as a function of its lipid composition ϕ. More explicitly, treating the mixed lipid layers as incompressible phases, let $F_{tot} = F(N,\phi) = N_B f_B(\phi_B) + N_I f_I(\phi_I)$ denote the Helmholtz free energy of a mixture containing $N = N^c + N^h$ molecules, of which $N^c = \phi N$ are cationic and $N^h = (1-\phi)N$ are electrically neutral helper co-lipids. Taking into account that when the transition takes place both phases coexist in solution

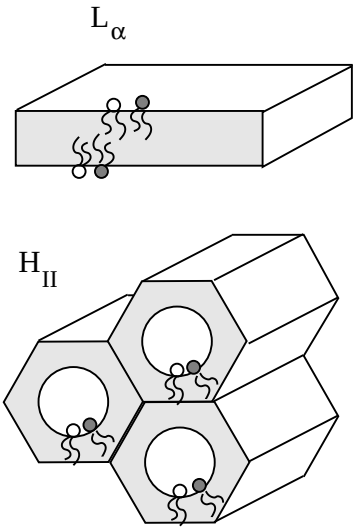

Figure 4: Schematic illustration of the planar bilayer (L_α) and inverse-hexagonal (H_{II}) phases. The shaded areas are the hydrophobic cores of the two phases, where individual lipid molecules adopt different packing geometries: cylindrical on average in the bilayer, and conical (widening from head to tail) in the inverse-hexagonal phase.

we use N_B and N_I ($N = N_B + N_I$) to denote the number of lipids in the bilayer and inverse-hexagonal phases, respectively; ϕ_B and ϕ_I are the compositions of the two phases and $f_B = F_B/N_B$ and $f_I = F_I/N_I$ denote the free energy per molecule in the two aggregation geometries; ($N_B\phi_B + N_I\phi_I = N\phi$). Minimizing F_{tot} with respect to $N_B^c = N_B\phi_B$ and $N_B^h = N_B(1-\phi_B)$, thus equating the chemical potentials of the cationic and helper lipids in both phases, we derive the phase coexistence equations, whose graphical solution corresponds to the "common tangent" construction, as illustrated somewhat later, in Fig. (**6**). First, however, let us consider in more detail the energetic and entropic contributions to, F (either F_B or F_I), the free energy of a mixed, partially charged, lipid aggregate of a given geometry.

Because of the very complex nature of inter-lipid interactions, the use of approximations in modeling F is inevitable. In many respects, averaging over some of the small scale (e.g., lipid headgroup fluctuations across the hydrocarbon-water interface) or large scale (e.g., long wavelength membrane undulations) is not only necessary, but actually desirable; their role in a mesoscopic phase transition such as the one of interest here is negligible. Such simplifications and approximations are legitimate not only in the selection of the relevant degrees of freedom but also in the level of the theoretical-computational treatment. Thus, for instance, atomic level computer simulations of the lamellar-hexagonal transition seem rather hopeless at present. On the other hand, while approximate, the mean field theoretical model outlined below captures all the essential physics of the problem. Furthermore, its extension to the more complex lipoplex problem is straightforward. Within this conception we express F as a sum of four principal contributions

$$F = F_c + F_v + F_m + F_e \tag{1}$$

The first term, F_c, is the curvature strain which accounts for deviations of the global packing symmetry of the lipid molecules from their optimal, "spontaneous", molecular packing geometry. The optimal packing geometry rarely coincides with the global aggregation symmetry. For instance, planar bilayers are often composed of lipids with slightly disparate headgroup and chain areas. Such lipids prefer the geometry of a weakly bent monolayer and their packing into a bilayer is thus a compromise involving a nonzero elastic strain energy.

A simple yet general and powerful formalism for treating curvature elastic deformations of lipid layers is due to Helfrich [53]. Using c_1 and c_2 to denote the two principal local curvatures at a given point of a lipid layer, ($R_i = 1/c_i; i = 1,2$ are the local radii of curvatures) the bending energy, F_c, of a lipid layer of total area A is expressed as,

$$F_c = \int_A da \left[\frac{k}{2}(c_1 + c_2 - c_0)^2 + \bar{k}c_1c_2\right] \tag{2}$$

with the integration extending over the entire membrane area A. The intrinsic elastic properties of the lipid molecules are embodied in the three material constants $k, \bar{k}$ and c_0. These are, the splay or bending modulus k and the saddle-splay or Gaussian modulus $\bar{k}$, which measure the rigidity of the lipid layer with respect to bending deformations, i.e., to deviations in membrane curvature away from the *spontaneous curvature*, c_0. Note that for both the L_α and H_{II} phases at least one main curvature vanishes so that the value of $\bar{k}$ is irrelevant here.

The crucial difference between the packing characteristics of the cationic lipid and the curvature loving co-lipid considered in the previous section is associated with their very different spontaneous curvatures. Whereas $c_0(\phi = 1) = c_0^c = 0$ for the pure cationic layer, $c_0(\phi = 0) = c_0^h$ is highly negative for the co-lipid ($c_0^h = -1/25$Å in the phase diagram of Fig. (**3**). For mixed layers, it is reasonable to assume that the spontaneous curvature varies linearly with composition, $c_0(\phi) = \phi c_0^c + (1-\phi)c_0^h$ [54, 55], and a constant bending rigidity $k(\phi) = k = 10k_BT$, the latter being a typical choice for lipid monolayers [56]; k_B is Boltzmann's constant and T the absolute temperature. With these considerations we have specified the composition dependence of $F_c(\phi)$. To apply Eq. 2, the curvatures of the respective lipid layer need to be measured at the so-called *neutral surface* [57]. (Measured with respect to this surface, bending and stretching deformations are decoupled.) The neutral surface is generally located close to the interfacial region, being planar for the L_α phase and of approximatively circular cross-section for the H_{II} structure.

The Helfrich free energy, Eq. 2, is in fact a series expansion of the curvature deformation energy in terms of the two principal curvatures, truncated beyond the quadratic terms. Thus, in principle, Eq. 2 is strictly applicable only for small curvature deformations. Yet, comparison with experiment supports its validity even for rather drastic bending deformations of lipid bilayers, such as those involved in the L_α-H_{II}, [58]. We also note that there is a recent alternative approach to account for the curvature strain of the H_{II} phase on the basis of a tilt deformation of the lipid layer [59, 60].

The second contribution, F_v, is only relevant for the H_{II} phase, representing the excess free energy of those lipid chains extending towards the interstitial sites of the hexagonal lattice [58, 61]. It augments the free energy per molecule in the H_{II} phase by about $0.35k_BT$.

The third contribution to F is the mixing free energy, F_m, of the lipid mixture which may be ideal or non-ideal, depending on the strength and nature of inter-lipid interactions.

The last contribution, F_e, is the electrostatic free energy. Both the L_α and H_{II} phases contain cationic lipids, whose electrostatic ("charging") free energies, $f_e^B = F_e^B/N_B$ and $f_e^I = F_e^I/N_I$ per molecule, depend on their interfacial curvatures and lipid compositions. One of the most common and useful, albeit approximate, approaches for calculating the electrostatic free energy of charged lipid layers (or, more generally, any macroion in electrolyte solution) is provided by Poisson-Boltzmann (PB) theory. This mean-field theory accounts for the balance between the two basic, but opposing, tendencies of the the mobile counterions in solution: (i) to closely associate with the surface charge (lipid charges in the present case) so as to minimize the Coulomb interaction energy, and, (ii) to disseminate into the aqueous solution thereby increasing their translational entropy.

This interplay between entropy and energy of the mobile counterions is simply reflected in the mathematical formulation of PB theory. That is, the free energy F_e is the (temperature weighted) sum of the electrostatic field energy, U_e, and the mixing entropy contribution, S. For a symmetric monovalent (1:1)

electrolyte solution it is given by

$$F_e = U_e + TS = \frac{\varepsilon}{2}\int_V dv(\nabla\Phi)^2 + k_BT\int_V dv\left[n_+\ln\frac{n_+}{n_0} + n_-\ln\frac{n_-}{n_0} - (n_+ + n_- - 2n_0)\right] \tag{3}$$

where n_+ and n_- are the local number densities of positively and negatively charged ions, respectively; n_0 is the corresponding ionic density in the bulk and ε is the dielectric constant of water. It is common to re-express the salt concentration, $n_0 = 1/(8\pi l_D^2 l_B)$, in terms of the Debye length, l_D, and the Bjerrum length, $l_B = e^2/(4\pi\varepsilon k_BT)$ where e denotes the elementary charge. In Eq. 3, $\nabla\Phi$ is the gradient of the electrostatic potential, Φ. Upon minimizing Eq. 3 with respect to the ionic densities one obtains the Boltzmann distributions $n_\pm = n_0\exp(\mp\Psi)$, expressed in terms of the reduced (dimensionless) electrostatic potential $\Psi = e\Phi/k_BT$. In combination with Poisson's equation, $\nabla\Phi = -\varepsilon e(n_+ - n_-)$, this gives rise to the familiar PB equation

$$l_D^2\nabla^2\Psi = \sinh\Psi \tag{4}$$

which is a second-order non-linear differential equation for the reduced potential Ψ.

Unfortunately, analytical solutions of the PB equation and the corresponding free energy, F_e, are available only for a few elementary cases [62]. For most systems the PB equation must be solved numerically, unless additional approximations are invoked. An important special case for which an analytical solution is available is that of a planar, uniformly charged, surface. The corresponding expression for the molecular free energy density is well known, and can serve as a model for a mixed planar layer composed of cationic and nonionic lipids. Assuming that both lipid species have the same cross-sectional area a_h per lipid headgroup, the electrostatic free energy, $f_e = u_e - Ts_e$, per molecule in a mixed layer containing a molar fraction, ϕ, of charged lipid is, [63]

$$\frac{f_e}{k_BT} = 2\phi\left[\frac{1-q}{p} + \ln(p+q)\right] \tag{5}$$

where $p = p_0\phi$, $p_0 = 2\pi l_B l_D/a_h$, and $q^2 = p^2 + 1$. For physiological salt solutions (where $l_D \approx 10$ Å) one finds $p_0 \approx 7$; the corresponding value for $l_D = 50$ Å is $p_0 \approx 35$.

For a weakly charged surface ($p \ll 1$) Eq. 5 reduces to the Debye-Hückel limit $f_e/k_BT = p_0\phi^2$. Here, the contributions from the electrostatic field energy and from the mixing entropy of the mobile ions are equally large; $u_e/k_BT = -s/k_B = p_0\phi^2/2$. More relevant for charged lipid membranes is the high charge limit ($p \gg 1$) where $f_e/k_BT = 2\phi[\ln(2p) - 1]$. Here the counterions are more closely associated with the macroion charges than is predicted in the Debye-Hückel regime. The electrostatic field energy is thus smaller and the entropic contribution larger than in the Debye-Hückel limit. Specifically, $-Ts/u_e = 2\ln(2p) - 3$ becomes large for large p. It follows that in the high charge regime the formation of a diffuse double layer induces mainly an immobilization of counterions, implying a severe entropy loss associated with the confinement to a narrow interfacial region of these, otherwise freely diffusing, ions.

Upon association of two oppositely charged macroions, electrical neutralization can be achieved through (partial, sometimes complete) compensation of their surface charges, enabling the liberation of the mobile ions back into the bulk solution thereby regaining their lost translational entropy. This *counterion release* process, pictorially illustrated in Fig. (**5**), is often the major driving force for the electrostatic association of oppositely charged macroions in solution. CL-DNA complex formation is one of the most striking examples of this phenomenon.

Though serving as the method of choice in most electrostatic problems involving macroions, like DNA, charged proteins and ionic lipid layers, it is important to remember the limits of validity of PB theory. Being a mean-field approach, PB theory neglects ion-ion correlations which seriously impairs its applicability to

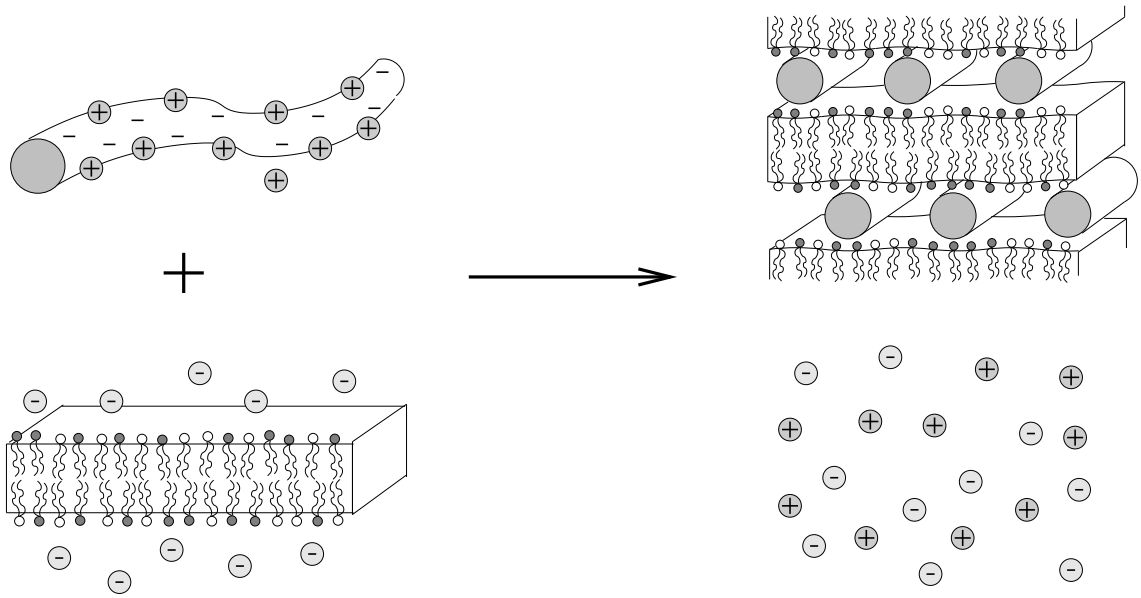

Figure 5: The release of counterions upon macroion association.

electrolyte solutions of higher valency than 1. Furthermore, PB theory treats all mobile ions as point charges, thus sometimes predicting unreasonably high local ion concentrations. Still, the theory captures correctly electrostatic energies for monovalent salt and not too highly charged macroions. Consequently, within PB theory the focus must be on 1:1 electrolytes and monovalently charged cationic lipids. The systems of interest in this review generally conform to these conditions.

Given the free energies of the two relevant phases, $F_B(N_B,\phi) = N_B f_B(\phi)$ and $F_I(N_I,\phi) = N_I f_I(\phi)$, the phase boundaries of the L_α-H_{II} transition can be determined using the common tangent construction, as illustrated in Fig. (**6**). This is a first order phase transition, implying a range of compositions, $\phi_I < \phi < \phi_B$, where the L_α and H_{II} structures coexist with fixed compositions ϕ_B and ϕ_I, respectively; $\phi = N^c/N$ denoting the overall mole fraction of cationic lipid in the system. For any given ϕ within the coexistence region, the relative proportions of molecules in the two phases, N_B/N_I are given, as usual, by the lever rule, $N_I(\phi - \phi_I) = N_B(\phi_B - \phi)$. For $\phi \leq \phi_I$, the system is monophasic with all lipids organized into the lower free energy H_{II} phase. Similarly, for $\phi \geq \phi_B$ the planar bilayer prevails.

Fig. (**6**) shows $f_B(\phi)$ and $f_I(\phi)$ for a lipid mixture composed of cationic lipids whose spontaneous curvature is $c_0 = 0$, and helper lipid for which $c_0 = -1/25\,\text{Å}$. The concentration of 1:1 electrolyte in solution is low, corresponding to a Debye-length of $l_D = 50\,\text{Å}$. For this system one finds $\phi_I = 0.02$ and $\phi_B = 0.08$. Fig. (**6**) displays a second set of calculated free energies, $f_B(\phi)$ and $f_I(\phi)$, corresponding to a similar lipid mixture but with the electrostatic interactions switched-off. This system is brought here to demonstrate the influence of electrostatic interactions on the lamellar-hexagonal transition, but may also be regarded as the high-salt limit of electrolyte solutions, where $l_D \to 0$ and all electrostatic interactions are fully screened. We note that in the electrically neutral system the coexistence region is shifted to significantly higher compositions ϕ_I and ϕ_B. For example, switching off electrostatic interactions at $\phi = 0.04$ would transform all lipids that reside in the L_α sub-phase back to a single H_{II} phase. In other words, the electrostatic interactions provide extra stabilization energy to the L_α over the H_{II} phase; consistent with the qualitative notion that the spatial confinement of the counterion cloud is more severe in the narrow circular tubes of the H_{II} phase as compared to the planar bilayer. This observation is confirmed by a recent experimental study of Lewis and McElhaney [64] who found that increasing the surface charge of mixed

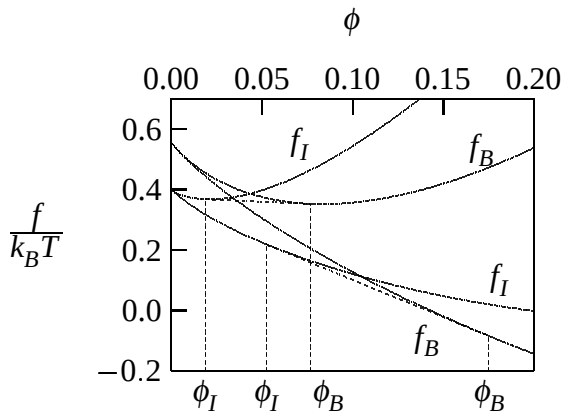

Figure 6: The free energies per lipid molecule, f_B and f_I, in the lamellar (L_α) and inverse-hexagonal (H_{II}) phases, respectively, as a function of the mole fraction of the cationic lipid, ϕ. The upper set of curves includes all free energy contributions; see Eq. 1. In the lower set the electrostatic contributions to f_B and f_I are omitted (that is, only the elastic, interstitial, and mixing contributions are included). The common tangent construction and the coexisting compositions, ϕ_I and ϕ_B, are marked by dashed lines for each set of curves. (adapted from Ref. [33], with permission).

cationic lipid layers indeed inhibits the formation of inverted non-lamellar phases.

4 The L_α^C-H_{II}^C transition of CL-DNA complexes

Having discussed the thermodynamics of the L_α-H_{II} transition, we now turn to consider the outcomes of adding dsDNA into an aqueous solution containing, as in the previous section, a mixture of cationic and curvature-loving helper lipid, at given composition ϕ. The phase behavior of this three component mixture is obviously richer and more challenging than that of the DNA-free system, as noted already in Sec. 2

Consider first a system containing just a small amount of added DNA, corresponding to the excess lipid regime, $\rho \gg 1$ in Fig. (**3**). The first question we would like to resolve pertains to the lipoplex structures appearing in the solution at any given ϕ. Because of the large excess of lipid molecules in solution the DNA can complex only a small fraction of these molecules. The composition of the remaining, uncomplexed, lipid mixture is practically unchanged, and should thus display the phase evolution expected for a DNA-free system. In particular, the phase boundaries, ϕ_I and ϕ_B, separating the monophasic H_{II} and L_α regions from the biphasic coexistence region, should coincide with those of the binary lipid mixture.

The formation free energies of the L_α^C and H_{II}^C complexes can be calculated using a (rather non-trivial) extension of the theoretical model outlined in the previous section. Postponing the discussion of these free energy calculations to the next section, we first show in Fig. (**7**) a schematic illustration of the phase evolution of a CL-DNA mixture as a function of ϕ, keeping ρ large and constant. The two shaded bars descibe the parallel evolution of lipoplex structures (top), and the excess (DNA-free) lipid structures (bottom), as ϕ increases at constant ρ. The calculated phase boundaries shown in the lower bar, $\phi_I = 0.02$ and $\phi_B = 0.08$, are indeed consistent with those obtained using the common tangent construction for the analogous, L_α-H_{II} transition, in the DNA-free system, as was shown in Fig. (**6**).

More interesting are the CL-DNA complexes. From the calculated results presented in the upper bar of

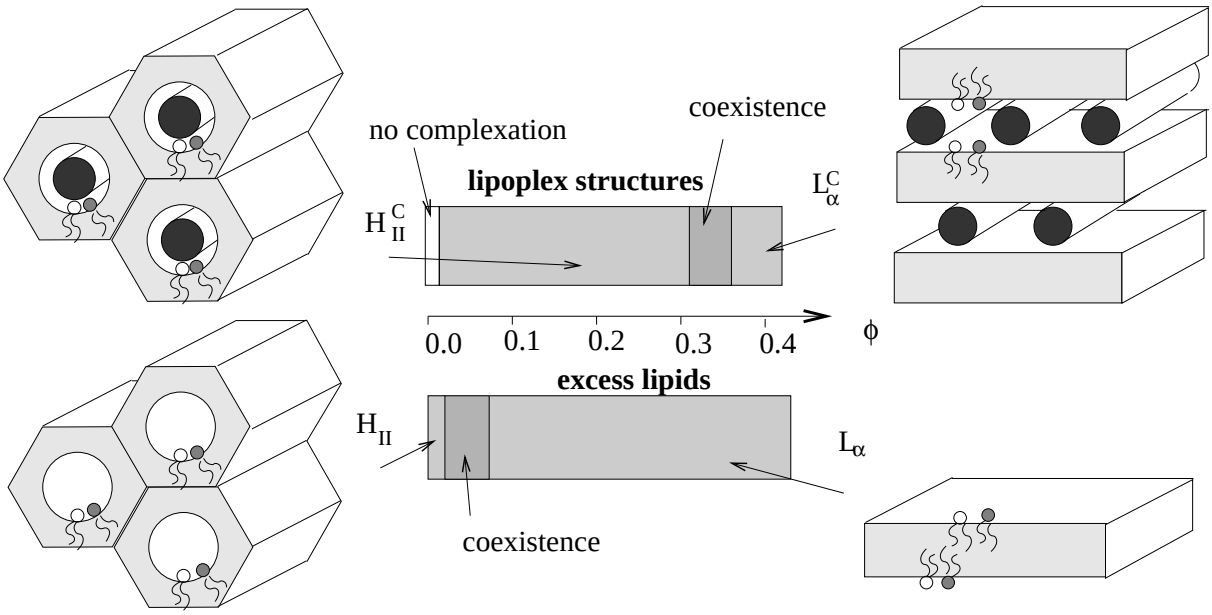

Figure 7: Structural evolution of lipid-DNA complexes and DNA-free lipid phases in a system containing a small amount of DNA and a large excess of the lipid mixture, shown as a function of the overall lipid composition ϕ. The lipid mixture involves bilayer-forming cationic lipids and curvature-loving helper lipids. The upper bar depicts the lipoplex H_{II}^{C}-L_{α}^{C} transition in the presence of excess lipid (large ρ regime in Fig. (**3**)), and the lower bar displays the corresponding transition, $H_{II} - L_{\alpha}$, in the lipid reservoir.

Fig. (**7**) we learn that no CL-DNA complex formation takes place in the narrow range of very small ϕ (in our specific example $\phi < 0.005$). This practically negligible composition regime is nevertheless interesting because it reflects the interplay between several competing free energy contributions which are relevant for all compositions. Explicitly, the lack of complex formation in the low ϕ limit can be explained as follows. Stable lipoplexes, either hexagonal or lamellar, show high stability around the isoelectric point but become rapidly unstable as their CL content deviates from this condition. Owing to the high charge density of dsDNA, isoelectricity requires sizable CL contents, e.g., $\phi \approx 0.35$ in the honeycomb structure. Thus, complex formation necessitates the transfer of CL molecules from their highly diluted lipid mixture to the concentrated enviroment of the complex. This disproportionation process involves a mixing free energy loss which at extremely low values of ϕ may inhibit the formation of complexes. However, as soon as ϕ begins increasing the electrostatic, complex formation, free energy becomes the dominant factor and lipoplexes appear in solution. It should be stressed that the lipid composition of the complexes, though not always isoelectric, is generally quite different from that of the original lipid mixture. Note also that ϕ in Fig. (**7**) refers to the overall mole fraction in solution, not in the lipoplex.

If ϕ remains sufficiently small (in our example $\phi < 0.3$) the stable lipoplex is the H_{II}^{C} structure. It involves double stranded DNA's intercalated within the aqueous tubes of an H_{II} phase. Most notably, the packing of the lipids is very similar in both the H_{II}^{C} and H_{II} phases. A cationic lipid mixture that alone has a strong preference for the inverted hexagonal, H_{II}, phase is consequently expected to form the H_{II}^{C} structure when exposed to DNA. However, from Fig. (**7**) we see that when ϕ reaches the $H_{II} - L_{\alpha}$ coexistence region, indicating identical stability of the two mixed lipid phases, the hexagonal complex still dominates. In fact, the hexagonal complex continues to prevail over the lamellar one even when the lipid reservoir becomes lamellar rather than inverse-hexagonal, at $\phi_B = 0.08$. (Lamellar lipoplexes appear and dominate once ϕ

exceeds 0.35.) The origin of this extended stability of the hexagonal complex is due to the essentially perfect electrostatic matching conditions provided by the concentric symmetry of the DNA and lipid surfaces.

Alternatively phrased, adding DNA to a mixed *planar* bilayer results in its *DNA-induced structural transition* into an *inverse-hexagonal* packing. In this connection it may be added that DNA is not the only macromolecule that is able to transform lipid phases. Some peptides like the cation-selective channel gramicidin A and other synthetic α-helical transmembrane peptides [65, 66, 67] reveal similar abilities. However, whereas hydrophobic interactions drive the L_α-H_{II} transition for the gramicidin A channel (which in fact is uncharged) DNA drives the structural transformation through its strong electrostatic interaction with the cationic lipids. The situation is at the first glance puzzling: DNA strongly interacts with cationic lipids that on their own have no tendency to form inverse-hexagonal structures. Adding DNA to a planar bilayer may induce the formation of the H_{II}^C phase even though additional cationic lipids enter the lipoplex (and thus would render the pure H_{II} phase even less stable). This points at the important role of the electrostatic interactions between DNA and cationic lipids that substantiall modify the lipid's preferred packing behavior.

5 Modeling the L_α^C and H_{II}^C structures

We are now ready to apply the theoretical tools discussed in Sec. 3 to model the L_α^C and H_{II}^C structures. Basically, the physical principles and modeling methods are the same, except for the fact that the number of degrees of freedom, both compositional and structural is larger, and the thermodynamic analysis is far more intricate.

The free energy of a solution containing DNA and a mixture of cationic and nonionic lipids can be expressed as a sum of the free energies corresponding to all structures that these components can form. A phase diagram such as the one shown in Fig. (**3**) is then derived by minimizing this free energy with respect to the exchange of molecules between phases, which is equivalent to equating the chemical potential of each of the three species in all coexisting phases. The input necessary for this calculation are the free energies of the five relevant phases, namely, the naked DNA whose free energy is simply proportional to its length, the bilayer and inverse-hexagonal phases of the binary lipid mixture which were treated in some detail in the previous section, and, of course, the sandwich and honeycomb complexes, to be discussed next.

We shall use $f_S = f_S(\phi, d)$ to denote the average free energy per lipid in a sandwich complex of composition ϕ and DNA-DNA spacing d. Changes in other structural variables of the complex, such as the thickness of the water gap, w, or of the lipid bilayer involve very high free energy costs, allowing to treat these variables as constants. Similarly, as discussed in Sec. 1, the thickness of the water gap in the honeycomb complex is practically constant, so that the average free energy per lipid in a honeycomb complex, $f_H = f_H(\phi)$, is only a function of its lipid composition. Given $f_S(d, \phi)$ and $f_H(\phi)$ and the free energies of the other three structures, the number and nature of the phases corresponding to a specific point, ρ, ϕ, in the phase diagram is derived by minimizing the overall free energy subject to the constraints of fixed ϕ and ρ and overall amount of material [33].

The L_α^C complex: The lamellar structure involves only flat lipid layers, (the influence of curvature modulations will be discussed in Sec. 6). Hence, only two contributions to F are relevant: the electrostatic free energy, $F_e(d, \phi)$, and the in-plane demixing free energy of the lipids, $F_m(d, \phi)$. (The interstitial energy is only relevant for the H_{II}-like lipid packing, and the elastic free energy can be set to zero which then serves as the reference state for bending deformations.)

Taking into account the periodicity and symmetry of the L_α^C structure, the electrostatic free energy of the complex can be evaluated by solving the PB equation, Eq. 4, within a quarter of a unit cell, as shown in Fig. (**8**). Furthermore, since the structure is translationally invariant along the DNA direction (z),

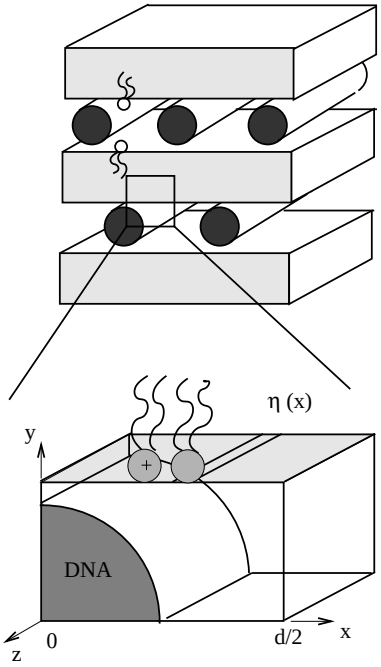

Figure 8: Schematic illustration of the L_α^C complex (left) and one-quarter of its unit cell (right) within which the PB equation was solved numerically [42]. The local composition $\eta(x)$ of the cationic lipid layer is allowed to adjust.

the electrostatic potential $\Psi(x,y)$ depends only on the x and y coordinates, and the PB equation is two- rather than three-dimensional. Three of the five boundary conditions for the PB equation, namely those corresponding to the virtual (water) surfaces in Fig. (**8**), follow from the symmetry of the L_α^C phase; e.g., the vanishing of $\partial\Psi/\partial x$ at $x = d/2$. Another boundary condition accounts for the charges on the DNA which is simply modeled as a uniformly charged cylinder.

The last boundary condition, concerning the cationic lipid surface, is the most complex and interesting one. Being a 2D *fluid* mixture, the lipid bilayer allows for lateral diffusion of the lipid molecules. In an isolated, mixed layer, the spatial distribution of the two lipid species will be, on average, uniform. On the other hand, the close proximity of oppositely (and highly) charged DNA rods can induce substantial spatial modulation (charge "polarization") of the cationic lipid distribution along the x-axis. The modulation of lipid charges is, of course, favored on electrostatic grounds, but involves a significant entropic penalty associated with the in-plane *demixing* of the lipid mixture. Denoting the local lipid composition along the x-axis by $\eta(x) = \eta$, the demixing free energy (conveniently measured per unit cell) is given by

$$F_m(d,\phi) = k_B T \left\langle \eta \ln \eta + (1-\eta)\ln(1-\eta) + \lambda(\phi - \eta) \right\rangle \tag{6}$$

with the angular brackets denoting averaging over the unit cell, and $\langle\eta\rangle = \phi$. The last term in Eq. 6 accounts for the conservation of the number of cationic lipids in the unit cell; λ is the corresponding Lagrange multiplier.

The next step is to express the free energy of the unit cell as a sum, $F = F_e + F_m$, of its electrostatic (Eq. 3) and lipid mixing (Eq. 6) contributions. Functional minimization of the total free energy with respect to the lipid composition profile $\eta = \eta(x)$ then yields a relation between η and the electrostatic potential, Ψ, namely

$$\eta = 1/(1 + e^{\Psi - \lambda}\,(1-\phi)/\phi) \tag{7}$$

This equilibrium profile enters the boundary condition, $(\partial\Psi/\partial y) = 2\eta p_0/l_D$, at the cationic lipid layer, which must be solved simultaneously and self-consistently with the PB equation. The PB equation satisfying these conditions and conserving the overall charge per unit cell can be solved numerically using a standard Newton-Raphson iteration scheme [42]. The result is the potential $\Psi(x,y)$ at any point within the aqueous part of the unit cell and the Lagrangian multiplier λ (see Eq. 6) which enables us to calculate from Eq. 7 the optimal compositional profile, $\eta(x)$.

In Fig. (**9**) we show the modulated composition profile for three different values of the average lipid composition ϕ. In all three cases the DNA-DNA spacing, $d^\star = d = a_h\phi/l$, corresponding to the "isoelectric" state, which is also the state of minimal free energy of the complex, (see below). The extent of lipid

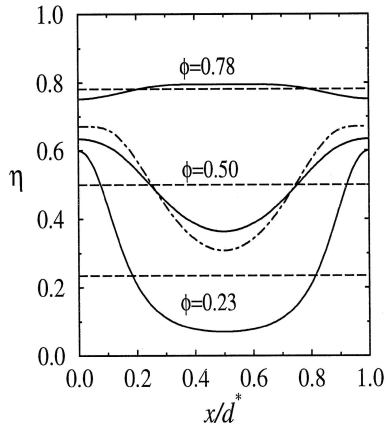

Figure 9: Spatial modulations of the cationic lipid charge within a unit cell of the L_α^C complex. The local mole fraction of cationic lipids, $\eta(x)$ (between two neighboring DNA strands), is shown (solid lines) for complexes of three lipid compositions: $\phi = 0.23$, 0.50, and 0.78. All complexes are at their isoelectric value of d. The horizontal (dashed) lines correspond to uniform charge densities. The dash-dotted line, corresponding to $\phi = 0.5$, shows the charge density profile in a (hypothetical) complex in which charge modulation (lipid demixing) does not involve any entropy penalty. Note that in all but the highest ϕ case, the cationic lipid tends to concentrate near the DNA rods, thus depleted from the center of the unit cell, (from Ref. [42], with permission).

"polarization" is very pronounced for small ϕ (and correspondingly large $d^\star$) where most cationic lipids accumulate near the DNA rods. The energetically optimal composition near the DNA rod, $\eta = a_h/2\pi R_D l = 0.65$, would lead to local charge matching between the DNA and the cationic layer. Despite the opposing effect of the lipid's demixing entropy, Fig. (**9**) clearly shows that for all three values of ϕ, the lipid layers attempt, quite successfully in fact, to adopt the "charge matching" composition $\eta = 0.65$ at $x = 0$ and $x = d^\star$. This also explains the behavior for large ϕ, where cationic lipids are actually depleted from the region close to the DNA.

After solving the PB equation we can return to $F(d,\phi) = F_e + F_m$ and calculate the formation free energy of the complex. Fig. (**10**) shows $F(d,\phi)$ as a function of ϕ for several values of the inter-axial spacing d. All free energy curves exhibit a minimum at, or very near, the isoelectric point where the sum of all lipid charges equals the number of DNA charges, implying $\phi = dl/a_h$. This result could in fact be anticipated, because perfect matching between the charges of two oppositely charged macroions allows the release of (previously confined) counterions into the aqueous solution. The corresponding gain in translational entropy of the mobile ions, which provides the ultimate driving force for the association of oppositely charged macroions, is then maximal. This general notion is certainly applicable in the case of the L_α^c complex. In

fact, a calculation of the enthalpic and entropic contributions to the free energy of L_α^C complex formation shows that the entropic contribution strongly dominates, being maximal (nearly 100 %) at the isoelectric point [68]. The entropic contribution can be translated into the number of counterions that are released into solution. This number has also been determined experimentally by conductivity measurements of CL-DNA solutions. Both theory and experiment show large – at the isoelectric point essentially complete – release of counterions [68, 40].

Comparison of the H_{II}^C complex with the L_α^C structure: In Sec. 3 we have analyzed the morphological transition from a planar bilayer (L_α) to the inverse-hexagonal (H_{II}) phase of a binary lipid mixture, finding that the relative stability of these phases is dominated by the different curvature strains (F_c) experienced by their constituent lipids. We also found that in cationic-nonionic mixtures the electrostatic interactions disfavor lipid packing in the H_{II} as compared to the L_α phases, thus shifting the coexistence region towards smaller values of ϕ; see Fig. (**6**). Yet, the driving force of the $H_{II} - L_\alpha$ transition in charged lipid layers is still the curvature strain, rather than electrostatic interactions.

The situation is markedly different for the $H_{II}^C - L_\alpha^C$ transition, where electrostatics is at least as important as the curvature elastic energy. As noted already in Fig. (**7**), the stability of the H_{II}^C complex, as compared to that of the H_{II} phase, is dramatically enhanced by the presence of the negatively charged DNA rods, residing in the water tubes of the inverse-hexagonal lipid array. In fact we have seen that for a wide range of overall lipid compositions, e.g., $\phi \leq 0.35$ for $\rho \gg 1$, as in Fig. (**7**), the honeycomb complex is more favorable than the planar sandwich complex, even when the raw lipid source is a planar bilayer. This special stability of the honeycomb complex reflects its highly favorable geometry, whereby the negatively charged DNA rod is tightly and symmetrically enveloped by the positively charged lipid interface. More precisely, this structure is particularly stable at the isoelectric point. The lipid composition ensuring isoelectricity depends on the thickness, δ, of the aqueous layer separating the DNA and lipid surfaces. For $\delta = 3$ Å, one finds $\phi \approx 0.35$, [30]; larger δ further decrease this value ($\phi \approx 0.3$ for $\delta = 6$ Å). Any deviation from isoelectricity involves a steep increase of the electrostatic free energy of the complex, F_e, as shown by the dashed curve in Fig. (**10**). In other words, whenever stable honeycomb complexes appear in solution, their lipid composition is nearly or exactly isoelectrical.

Like the honeycomb complexes, the sandwich complexes also tend to be isoelectric. Since the total cationic charge per unit cell of the lamellar complex is proportional to $d\phi$, the lipid composition ensuring isoelectricity is inversely proportional to the DNA-DNA spacing d. In addition to the electrostatic energy of the honeycomb complex, Fig. (**10**) shows also the electrostatic free energy of the lamellar complex, as obtained by numerical solution of PB equation, for several values of d. The minima of F_e are indeed located at (or very near) the isoelectric point, i.e., at $\phi \propto 1/d$. Note, however, that these minima are higher and shallower than the minimum in the electrostatic free energy of the honeycomb complex. This relative "softness" of the lamellar complex is a direct consequence of its lower symmetry and less "compact" DNA-lipid contact in comparison to the honeycomb complex. Also, the less stringent packing restrictions imposed on this structure allow variations in d (even at constant ϕ, implying deviations from isoelectricity) at a rather small free energy cost. This additional degrees of freedom of the lamellar structure explains its abundance in various regions of lipoplex phase diagrams, even in systems with high content of curvature-loving lipids; see Fig. (**3**).

6 Curvature modulations within the L_α^C complex

Treating the lipid layers in the L_α^C complex as perfectly planar is rigorously appropriate only in the limit of very stiff membranes with a correspondingly high bending constant, k (see Eq. 2). In this limit, the energetic penalty associated with any elastic membrane deformation would be prohibitively high. Typically,

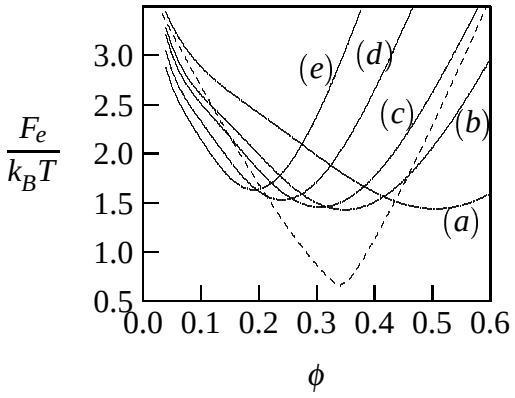

Figure 10: The electrostatic free energy per unit cell of the L_α^C complex (per 1 Å length of DNA), as a function of the CL mole fraction, ϕ. The solid curves correspond to five representative values of DNA-DNA spacing: $d = 35.0$ Å (a), $d = 51.8$ Å (b), $d = 59.7$ Å (c), $d = 77.0$ Å (d), and $d = 97.4$ Å (e). We also show (dashed line) the electrostatic energy of the H_{II}^C complex. Note that d determines the number of lipid molecules in the L_α^C complex. The solid curve (c) and the dashed line correspond to the same number of molecules (per unit DNA length) in the lamellar and hexagonal complexes, respectively, (from Ref. [33], with permission).

however, the bending rigidities of lipid membranes are $k \approx 10 k_B T$, implying that curvature fluctuations within the lamellar comlex cannot be ruled out. The DNA lattice may actually enhance the appearance of periodic membrane undulations, as illustrated in Fig. (**11**). When coupled to correlated modulations in lipid composition these curvature modulations may well represent the equilibrium structure of the complex. As the amplitude of these modulations increases, 3D order may set in the lipid-DNA array, whereby DNA monolayers in adjacent galleries become spatially correlated with each other.

The spatial "locking" of neighboring DNA galleries can affect the membrane-to-membrane repeat distance, h. Thus, for example, in the multilamellar 3D array depicted in Fig. (**11**) the repeat distance, $h < h^\star$, is smaller then the corresponding value, $h^\star$, for the perfectly planar lamellar complex. The curvature modulations have thus lead to a compression of the lamellar complex. In principle, the opposite behavior, describing swelling of the L_α^C complex ($h > h^\star$) is also possible. Indeed, swelling has been observed for a lamellar (L_α^C-like) phase made of cationic lipids, neutral co-lipids, and the anionic polypeptide poly-L-glutamic acid [69].

Unequivocal evidence for spatial correlations between adjacent DNA galleries has been reported in a recent X-ray study [70]. It should be noted, however, that the lipid layers in this study were in the crystalline ("gel") phase (L_β^C) rather than in the fluid ("liquid-crystalline", L_α^C) state. Strong indications for inter-gallery locking in lipoplexes involving fluid lipid membranes, has recently been presented based on cryo-TEM measurements [71].

At least three different theoretical approaches have been proposed for modeling curvature modulations in the L_α^C complex. In one model the bending modulations of the lipid layers are not merely supplementary to the dominating electrostatic interactions but play a crucial role in determining the DNA-DNA distance, d, within each gallery. This model, suggested by Dan [72, 73], postulates a competition between elastic attraction and electrostatic repulsion between neighboring DNA strands. The membrane-mediated DNA-DNA attraction is explained using membrane elasticity theory, as originally proposed for modeling the

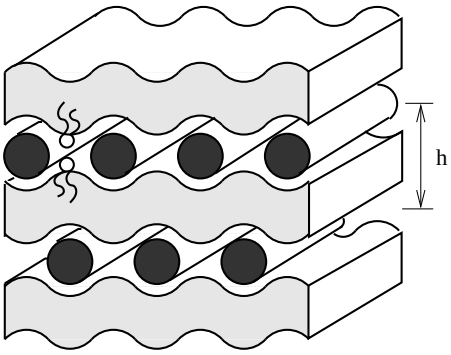

Figure 11: Schematic illustration of curvature modulations within the sandwich-like (L_α^C) complex. The lamellar repeat distance is denoted by h. The weakly shaded areas represent hydrocarbon chain regions of the involved lipid layers. The solid circles indicate DNA cross-sections. Some lipids are shown schematically.

interaction between hydrophobic inclusions, like integral proteins or peptides [74]. Within this model each DNA strand induces a localized elastic bending deformation, and interference of the bending deformations of neighboring DNA strands gives rise to attractive interactions between adjacent DNA's. These indirect, membrane-mediated interactions compete with the direct electrostatic DNA-DNA repulsion which then leads to an equilibrium distance between neighboring DNA strands. The model of Dan predicts a finite equilibrium distance not only for the DNA rods in the L_α^C phase but also for dsDNA adsorbed onto an isolated lipid bilayer. An AFM study of DNA adsorption onto a supported cationic lipid membrane suggests the possible existence of attractive forces between neighboring DNA molecules [75]. Elastic, membrane-mediated, interactions could also contribute to the condensation of DNA adsorbed on cationic membranes in the presence of divalent electrolyte counterions [76].

At this point it should be noted that elastic membrane deformation are not the only mechanism of lipid-mediated attraction between adsorbed macromolecules. Attraction between adsorbed macroions (like DNA or proteins) can also take place in elastically unperturbed membranes, provided the lipid mixture constituting the membrane is non-ideal. That is, if attractive interactions between lipids of the same species are stronger than those between different species there will be an effective attraction between membrane-adsorbed macroions which may be strong enough to induce lateral phase separation of a macroion-decorated mixed lipid membrane [77]. The origin of this attraction is the gradient in lipid composition around the macroion's adsorption zone and, consequently, the unfavorable lipid-lipid interaction ("line") energy across the boundary of this zone [78].

Another theoretical analysis of inter-membrane correlations in the L_α^C structure was presented by Schiessel and Aranda-Espinoza [79]. Based on linearized PB theory the authors have analyzed how the electrostatic interaction between DNA rods and (initially planar) cationic membranes affects the equilibrium value of the interlayer distance h in the L_α^C structure. Treating the L_α^C complex as electrostaticially transparent, the full electrostatic coupling of the membrane stack and the intercalated DNA galleries had to be considered, including all membrane-membrane, membrane-rod, and rod-rod interactions. It was found that the electrostatic interactions generally favor compression of the lamellar complex ($h - h^\star < 0$); yet, the magnitude of the compression is estimated to be quite small, on the order of $h - h^\star \approx -1$ Å.

A detailed theoretical analysis of curvature modulations in the L_α^C phase was also provided by Harries et al [80]. The approach is based on the solution of the non-linear PB equation within the unit cell of the L_α^C structure. The unit cell is analogous to the one shown in Fig. (**8**), but allows for a sinusoidal curvature modulation of the lipid interface. The wavelength of the modulation is set equal to $2d$ and its amplitude is

derived by minimizing the free energy of the complex. All other relevant features, like the low dielectric constants inside the DNA rod and the membrane, the adjustability of the DNA-DNA distance d, and the mobility of the membrane lipids (and hence a modulation of ϕ), are self-consistently incorporated into the model. The results show strong correlations between curvature and composition modulations, and a tendency of the cationic membranes to partially wrap around the DNA rods, corresponding to a compression of the complex ($h - h^\star < 0$). The degree of compression (or, equivalently, the amplitude of the sinusoidal deformation) depends on the composition-dependent material properties of the cationic lipid membrane. For typical bending rigidities of the lipid layer, say $k \approx 10 k_B T$, the curvature modulations are quite small, $|h - h^\star| \approx 1 \ldots 2$ Å. However, for softer lipid layers ($k \approx 1 k_B T$) and large DNA-DNA spacing d, the amplitude of curvature modulation can be as high as 10 Å. Under these conditions the curvature moduluation-induced energy gain per persistence length of DNA is much larger than $k_B T$, and 3D ordering of the lipid-DNA array (i.e., monolayer locking) is the equilibrium configuration.

Correlations between the DNA galleries within the L_α^C structure are also of fundamental physical interest. Within each gallery, the array of aligned DNA molecules constitutes a two-dimensional smectic [28]. Without coupling between the DNA galleries, thermal fluctuations would destroy any true long-range order within these two-dimensional smectics. On the other hand, for sufficiently strong coupling a columnar lattice would appear which re-establishes long-range order [70]. Most interestingly, in between–for weak coupling–a new "sliding" columnar phase with orientational long-range order but short-range positional order has been postulated [81, 82, 83, 41]. Whether the L_α^C structure can be viewed as an experimental realization of the sliding columnar phase is still an unsettled question.

7 CL-DNA phase diagrams: role of the co-lipid

In Sec. 2 we have discussed a generic CL-DNA phase diagram for a curvature-loving co-lipid, like the commonly used lipid DOPE. Other types of lipid mixture have also been tested and used; e.g., a lipid mixture in which the planar bilayer is the spontaneous aggregation geometry of both the cationic and helper lipid [18]; i.e., $c_0 \approx 0$ for both lipid components. In this section we shall first discuss in some detail the (relatively simple) phase behavior of such a mixture, and conclude with a brief analysis of the phase behavior corresponding to "very soft" lipid mixtures, (i.e., of low bending rigidity k). Both types of systems have been studied experimentally, see e.g., [18, 19].

Bilayer-forming co-lipid: The use of a bilayer-loving co-lipid (such as PC's) typically prevents the formation of any non-bilayer lipid structures. That is, both the inverse-hexagonal, H_{II}, phase and the corresponding H_{II}^C lipoplex are no longer possible. Instead, all lipid layers remain in their planar configuration, independent of their composition ϕ. It should be noted, however, that H_{II}^C complex formation is nevertheless possible, provided k is very small ($k \approx 1 k_B T$), as discussed later in this section. For typical bending rigidities ($k \approx 10 k_B T$), nonlamellar structures can be ruled out, and only L_α^C lipoplexes are relevant.

The structural characteristics of the L_α^C complex have been carefully studied and systematically analysed as a function of lipid composition, salt content and additional parameters, using X-ray and other techniques [18, 20, 84, 85]. Perhaps the most remarkable finding of this structure is the adjustability of the DNA-DNA distance d, which is intimately related to the overall phase behavior and can be rationalized [42, 86] within the theoretical framework discussed in Sec. 5.

In Fig. (**12**) we show a theoretical phase diagram, calculated for a lipid mixture with zero spontaneous curvature of both lipids, $c_0^c = c_0^h = 0$, implying $c_0(\phi) = c_0^c + \phi(c_0^h - c_0^c) = 0$ for the lipid mixture regardless of ϕ. Provided the lipid mixture is not too soft, (our calculations predict $k \geq 4 k_B T$) this phase diagram is independent of the bending rigidity k.

The gross features of the phase evolution as a function of the lipid-to-DNA charge ratio, ρ, at a given

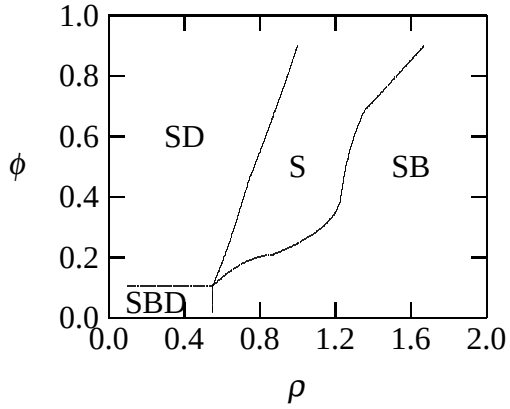

Figure 12: Generic phase diagram of a lipid-DNA mixture involving lipids which self-assemble into rigid planar membranes, calculated as a function of the mole fraction of the cationic lipid, ϕ, and the lipid-to-DNA charge ratio ρ.. The symbols *S*, *B*, and *D* denote, respectively, the L_α^C, L_α and uncomplexed (naked) DNA phases. (from Ref. [33], with permission).

overall lipid composition ϕ ($0.2 \lesssim \phi \lesssim 0.8$) are easily understood. These features are pictorially illustrated in Fig. (**13**), which also shows how d varies with ρ. As expected, CL-DNA complexes begin appearing in solution as soon as liposomes are added to the system.

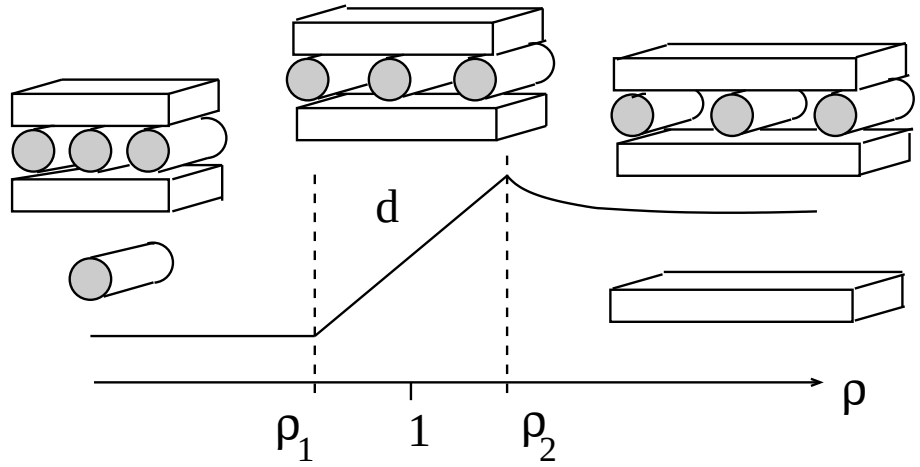

Figure 13: Schematic illustration of the phase behavior in a solution containing lamellar CL-DNA complexes. The DNA-DNA distance, d, is schematically shown as a function of the lipid-to-DNA charge ratio, ρ.

For small lipid-to-DNA ratios, $\rho < \rho_1$, only part of the DNA can be complexed, so that naked DNA coexists with L_α^C lipoplexes, in which the dsDNA rods within a lipid gallery are densely packed. The small d values in this regime reflect the tendency of the highly charged DNA rods to insert into the lipid array and thus reduce the electrostatic free energy of the system. This tendency is strong enough to induce "negative overcharging" of the complex; i.e., d is smaller than its value at the isoelectric point ($d = d^\star = a_h\phi/l$). This overcharging process must involve the immobilization of a corresponding number of previously mobile

cations from the aqueous solution, in order to preserve the overall electroneutrality of the complex. The L_α^C complex tolerates this entropically less favorable state in compensation for the additional amount of complexed DNA, and the corresponding gain of electrostaic free energy.

As ρ continues to increase the point, $\rho = \rho_1$, is reached where all DNA becomes complexed, and newly added lipids are all incorporated into the sandwich complex. The system thus proceeds through a single phase region where $d(\rho)$ increases linearily with ρ. The single phase region, $\rho_1 \leq \rho \leq \rho_2$, includes the isoelectric point $\rho = 1$. Upon crossing this point the L_α^C structure changes from negative to positive overcharging. Again, positively overcharged L_α^C complexes need to immobilize anions from the salt solution and are thus not in their optimal energetic state. Yet, this is still more favorable than expelling all excess lipids and forming an extra cationic bilayer that itself would have to immobilize salt ions. As ρ approaches ρ_2 newly added lipids still enter the sandwich but tend to evade into the membrane regions between the DNA strands. There, they are increasingly less effective in interacting with the DNA strands. Instead, they increase inter-bilayer repulsion by interacting among each other. Consequently, at some specific, sufficiently large, $\rho = \rho_2$ the system phase separates again, and a planar excess bilayer is formed. Note that this excess bilayer need not have the same composition as the L_α^C complex. In fact, due to compositional adjustability of the L_α^C and L_α phases, the theoretical treatment predicts a slight decrease in d with ρ for $\rho > \rho_2$, [42].

Soft membranes: We have seen how manipulation of the preferred packing geometry of the lipid layer affects lipoplex structure. Experimental evidence shows yet another way: membrane softening (i.e., lowering k) by addition of an appropriate cosurfactant like a short chain alcohol [19]. The addition of cosurfactnat may have little effect on the preferred packing geometry (i.e., spontaneous curvature) of the lipid mixture, but it costs now much less energy to shift the actual packing geometry away from the preferred one. The elastic free energy in Eq. 2 underlines the physical origin of this mechanism: membrane softening corresponds to a decrease in the bending constant k. The spontaneous curvature c_0 is then less important for the actual phase behavior of the CL-DNA mixture. Instead, electrostatic interactions become the dominating contribution to the free energy. Recall from our discussion of Fig. (**10**) the subtle interplay between the two lipoplex geometries: The energetically optimal but compositionally constrained H_{II}^C structure, versus the energetically less favorable yet adjustable L_α^C complex. This suggests the appearance of both the L_α^C and H_{II}^C structures (separately and in coexistence) in various regions of the phase diagram, as corroborated by the theoretical results shown in Fig. (**14**).

Similarly to Fig. (**3**) we note the appearance of the L_α^C-H_{II}^C transition. As expected the transition can be induced by adding the membrane softening "co-lipid" (which need not be a lipid) to the CL-DNA mixture at the isoelectric point, $\rho = 1$. (The corresponding path in the phase diagram for this "dilution" experiment starts at $\phi \approx 1$ and proceeds towards smaller ϕ at $\rho = 1$.) Indeed, this is what has beed observed experimentally by adding a short chain amphiphile to the lipid mixture [19].

8 Concluding remarks

Our concrete goal in this review has been to highlight the physical mechanisms underlying the formation of lipid-DNA complexes in aqueous electrolyte solution, to analyze their structure as a function of lipid composition and DNA-to-lipid ratio, and to feature the very rich phase behavior of these practically and theoretically important systems. Starting with a rather complex phase diagaram, we have gradually unfolded the relevant thermodynamic and structural degrees of freedom governing the phase behavior of the multicomponent system. Particular emphasis has been given to the complementary, sometimes competing, roles of lipid chain packing on the one hand, and electrostatic DNA-lipid interactions on the other hand. We have also discussed, albeit briefly, the power and limitations of the theoretical tools used in our analysis.

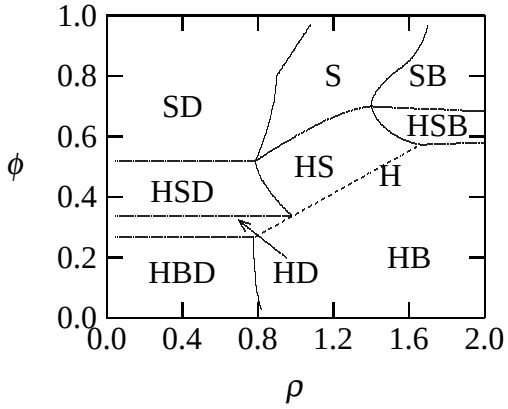

Figure 14: Phase diagram of a lipid-DNA mixture, for lipids which self-assemble into very soft planar membranes, calculated as a function of the mole fraction of the cationic lipid, ϕ, and the lipid-to-DNA charge ratio ρ. The symbols *S*, *H*, *B*, *I* and *D* denote, respectively, the L_α^C, H_{II}^C, L_α, H_{II}^C, and uncomplexed (naked) DNA phases. The straight dashed line marks the single H_{II}^C phase region (from Ref. [33], with permission).

Related to the last point above, we had another, more general, objective in this review: to convince the reader that theoretical modeling of a seemingly very complex thermodynamic-biophysical system is not necessarily hopeless. In fact, by a judicious choice of the theoretical tools, and proper identification of the most relevant (often the experimentally controllable) degrees of freedom, the theoretical modeling can provide not only *post factum* interpretations of experimental observations, but also nontrivial *a-priori* useful predictions.

Acknowledgment

We thank Cyrus Safinya, Joachim Rädler, Chezy Barenholz, Ishi Talmon, Bill Gelbart and Robijn Bruinsma for many illuminating discussions in the course of the last several years. Particular thanks are due to Daniel Harries who was a principal collaborator in most of the theoretical work outlined in this review. SM thanks the support of the Türinger Ministerium für Wissenschaft, Forschung und Kunst. ABS thanks the financial support of the Israel Science Foundation and the US-Israel Binational Science Foundation. The Fritz Haber center, where much of the theoretical work reported here was performed, is supported by the Minerva Foundation, Munich, Germany.

References

[1] Felgner, P. L. *Scientific American*, **1997**, *276*, 102.

[2] Kamiya, H.; Tsuchiya, H.; Yamazaki, J.; Harashima, H. *Adv Drug Deliv Rev.*, **2001**, *52*, 153.

[3] Audouy, S.; Hoekstra, D. *Molecular Membrane Biology*, **2001**, *18*, 129.

[4] Ferrari, M. E.; Rusalov, D.; Enas, J.; Wheeler, C. J. *Nucl. Acid. Res.*, **2002**, *30*, 1808.

[5] Ferrari, M. E.; Rusalov, D.; Enas, J.; Wheeler, C. J. *Nucl. Acid. Res.*, **2001**, *29*, 1539.

[6] Cornelis, S.; Vandenbranden, M.; Ruysschaert, J. M.; Elouahabi, A. *DNA and Cell Biology*, **2002**, *21*, 91.

[7] Colin, M.; Moritz, S.; Fontanges, P.; Kornprobst, M.; Delouis, C.; Keller, M.; Miller, A. D.; Capeau, J.; Coutelle, C.; Brahimi-Horn, M. C. *Gene Therapy*, **2001**, *8*, 1643.

[8] Dass, C. R. *J. Pharm. Pharmacol.*, **2002**, *54*, 593.

[9] Langner, M. *Cell. Mol. Biol. Lett.*, **2000**, *5*, 295.

[10] Dias, R.; Antunes, F.; Miguel, M.; Lindman, S.; Lindman, B. *Braz. J. Med. Biol. Res.*, **2002**, *35*, 509.

[11] Seddon, J. M.; Templer, R. H. In *Structure and Dynamics of Membranes*; Lipowsky, R.; Sackmann, E., Ed.; Elsevier: Amsterdam, **1995**; Vol *1*, pp. 98–160.

[12] Felgner, P. L.; Ringold, G. M. *Nature*, **1989**, *331*, 461.

[13] Gershon, H.; Ghirlando, R.; Guttman, S. B.; Minsky, A. *Biochemistry*, **1993**, *32*, 7143.

[14] Gustafsson, J.; Arvidson, G.; Karlsson, G.; Almgren, M. *Biophys. Biochim. Acta.*, **1995**, *1235*, 305.

[15] Tarahovsky, Y. S.; Khusainova, R. S.; Gorelov, A. V.; Nicolaeva, T. I.; Deev, A. A.; Dawson, A. K.; Ivanitsky, G. R. *FEBS Lett.*, **1996**, *390*, 133.

[16] Sternberg, B.; Sorgi, F. L.; Huang, L. *FEBS Lett.*, **1994**, *356*, 361.

[17] Sternberg, B. *J. Liposome Res.*, **1996**, *6*, 515.

[18] Rädler, J. O.; Koltover, I.; Salditt, T.; Safinya, C. R. *Science*, **1997**, *275*, 810.

[19] Koltover, I.; Salditt, T.; Rädler, J. O.; Safinya, C. R. *Science*, **1998**, *281*, 78.

[20] Lasic, D. D.; Strey, H.; Stuart, M. C. A.; Podgornik, R.; Frederik, P. M. *J. Am. Chem. Soc.*, **1997**, *119*, 832.

[21] Dias, R. S.; Lindman, B.; Miguel, M. G. *J. Phys. Chem. B.*, **2002**, *106*, 12600.

[22] Uhrikovi, D.; G, G. Rapp; Balgavy, P. *Bioelectrochemistry*, **2002**, *58*, 87.

[23] Caracciolo, G.; Caminiti, R.; Natali, F.; Castellano, A. C. *Chem. Phys. Lett.*, **2002**, *366*, 200.

[24] Hui, S. W.; Langner, M.; Zhao, Y-L.; Patrick, R.; Hurley, E.; Chan, K. *Biophys. J.*, **1996**, *71*, 590.

[25] Kim, T. W.; Kim, Y. J.; Chung, H.; Kwon, I. C.; Sung, H. C.; Jeong, S. Y. *J. Control. Release*, **2002**, *21*, 455.

[26] Zuhorn, I. S.; Oberle, V.; Visser, W. H.; Engberts, J. B. F. N.; Bakowsky, U.; Polushkin, E.; Hoekstra, D. *Biophys. J.*, **2002**, *83*, 2096.

[27] Wiethoff, C. M.; Gill, M. L.; Koe, G. S.; Koe, J. G.; Middaugh, C. R. *J. Biol. Chem.*, **2002**, *277*, 44980.

[28] Salditt, T.; Koltover, I.; Rädler, J. O.; Safinya, C. R. *Phys. Rev. Lett.*, **1997**, *79*, 2582.

[29] Salditt, T.; Koltover, I.; Rädler, J. O.; Safinya, C. R. *Phys. Rev. E*, **1998**, *58*, 889.

[30] May, S.; Ben-Shaul, A. *Biophys. J.*, **1997**, *73*, 2427.

[31] Sternberg, B. In *Medical applications of liposomes*; Lasic, D. D.; Papahadjopoulos, P., Ed.; Elsevier: Amsterdam, **1998**; Vol *1*, pp. 395–427.

[32] Hope, M. J.; Mui, B.; Ansell, S.; Ahkong, Q. F. *Molecular Membrane Biology*, **1998**, *15*, 1.

[33] May, S.; Harries, D.; Ben-Shaul, A. *Biophys. J.*, **2000**, *78*, 1681.

[34] Bandyopadhyay, S.; Tarek, M.; Klein, M. L. *J. Phys. Chem. B*, **1999**, *103*, 10075.

[35] Pink, D. A.; Quinn, B.; Moeller, J.; Merkel, R. *Phys. Chem. Chem. Phys.*, **2000**, *2*, 4529.

[36] Ryhänen, R. J.; Säily, M. J.; Paukku, T.; Borocci, S.; Mancini, G.; Holopainen, J. M.; Kinnunen, P. K. J. *Biophys. J.*, **2002**, *84*, 578.

[37] Seelig, J.; Gally, G. U.; Wohlgemuth, R. *Biophys. Biochim. Acta.*, **1977**, *467*, 109.

[38] Scherer, P. G.; Seelig, J. *Biochemistry*, **1989**, *28*, 7720.

[39] Zantl, R.; Baicu, L.; Artzner, F.; Sprenger, I.; Rapp, G.; Rädler, J.O. *J. Phys. Chem. B*, **1999**, *103*, 10300.

[40] Simberg, D.; Danino, D.; Talmon, Y.; Minsky, A.; Ferrari, M. E.; Wheeler, C. J.; Barenholz, Y. *J. Biol. Chem.*, **2001**, *276*, 47453.

[41] Golubovic, L.; Lubensky, T. C.; O'Hern, C. S. *Phys. Rev. E*, **2000**, *62*, 1069.

[42] Harries, D.; May, S.; Gelbart, W. M.; Ben-Shaul, A. *Biophys. J.*, **1998**, *75*, 159.

[43] Menes, R.; Pincus, P.; Pittman, R.; Dan, N. *Europhys. Lett.*, **1998**, *44*, 393.

[44] Bruinsma, R.; Mashl, J. *Europhys. Lett,*, **1998**, *41*, 165.

[45] Kuhn, P. S.; Barbosa, M. C.; Levin, Y. *Physica A*, **1999**, *269*, 278.

[46] Kuhn, P. S.; Barbosa, Y. Levinand M. C. *Physica A*, **1999**, *274*, 8.

[47] Podgornik, R. *Langmuir*, **1997**, *13*, 4791.

[48] Schiessel, H. *Eur. Phys. J. B*, **1998**, *6*, 373.

[49] Grosberg, A. Y.; Nguyen, T. T.; Shklovskii, B. I. *Mod. Rev. Phys.*, **2002**, *74*, 329.

[50] Zuhorn, I. S.; Hoekstra, D. *J. Membr. Biol.*, **2002**, *189*, 167.

[51] Smisterova, J.; Wagenaar, A.; Stuart, M. C.; Polushkin, E.; ten Brinke, G.; Hulst, R.; Hoekstra, J. B. Engberts D. *J. Biol. Chem*, **2001**, *276*, 47615.

[52] Mui, B.; Chow, Q. F. Ahkong L.; ; Hope, M. J. *Biophys. Biochim. Acta.*, **1998**, *1467*, 281.

[53] Helfrich, W. *Z. Naturforsch.*, **1973**, *28*, 693.

[54] May, S.; Ben-Shaul, A. *J. Chem. Phys.*, **1995**, *103*, 3839.

[55] Andelman, D.; Kozlov, M. M.; Helfrich, W. *Europhys. Lett.*, **1994**, *25*, 231.

[56] Niggemann, G.; Kummrow, M.; Helfrich, W. *J. Phys. II France*, **1995**, *5*, 413.

[57] Kozlov, M. M.; Winterhalter, M. *J. Phys. II France*, **1991**, *1*, 1077.

[58] Kozlov, M. M.; Leikin, S.; Rand, R. P. *Biophys. J.*, **1994**, *67*, 1603.

[59] Hamm, M.; Kozlov, M. M. *Eur. Phys. J. B*, **1998**, *6*, 519.

[60] May, S.; Ben-Shaul, A. *Biophys. J.*, **1999**, *76*, 751.

[61] Gawrisch, K.; Parsegian, V. A.; Hajduk, D. A.; Tate, M. W.; Gruner, S. M.; Fuller, N. L.; Rand, R. P. *Biochemistry*, **1992**, *31*, 2856.

[62] Andelman, D. In *Structure and Dynamics of Membranes*; Lipowsky, R.; Sackmann, E., Ed.; Elsevier: Amsterdam, **1995**; Vol *1*, pp. 603–642.

[63] Evans, D. F.; Wennerström, H. *The colloidal domain, where physics, chemistry, and biology meet*. VCH publishers, 2nd Ed., **1994**.

[64] Lewis, R. N. A. H.; McElhaney, R. N. *Biophys. J.*, **1999**, *79*, 1455.

[65] Killian, J. A.; Salemink, I.; de Planque, M. R. R.; Lindblom, G.; Koeppe, R. E.; Greathouse, D. V. *Biochemistry*, **1996**, *35*, 1037.

[66] Morein, S.; Strandberg, E.; Killian, J. A.; Persson, S.; Arvidson, G.; Koeppe, R. E.; Lindblom, G. *Biophys. J.*, **1997**, *73*, 3078.

[67] van der Wel, P. C. A.; Pott, T.; Morein, S.; Greathouse, D. V.; Koeppe, R. E.; Killian, J. A. *Biochemistry*, **2000**, *39*, 3124.

[68] Wagner, K.; Harries, D.; May, S.; Kahl, V.; Rädler, J. O.; Ben-Shaul, A. *Langmuir*, **2000**, *16*, 303.

[69] Subramanian, G.; Hjelm, R. P.; Deming, T. J.; Smith G. S.; Li, Y.; Safinya, C. *J. Am. Chem. Soc*, **2000**, *122*, 26.

[70] Artzner, F.; Zantl, R.; Rapp, G.; Rädler, J.O. *Phys. Rev. Lett.*, **1998**, *81*, 5015.

[71] Battersby, B. J.; Grimm, R.; Hübner, S.; Cevc, G. *Biophys. Biochim. Acta.*, **1998**, *1372*, 379.

[72] Dan, N. *Biophys. J.*, **1996**, *71*, 1267.

[73] Dan, N. *Biophys. J.*, **1997**, *73*, 1842.

[74] Dan, N.; Pincus, P.; Safran, S. A. *Langmuir*, **1993**, *9*, 2768.

[75] Fang, Y.; Yang, J. *J. Phys. Chem. B*, **1997**, *101*, 441.

[76] Koltover, I.; Wagner, K.; Safinya, C. *Proc. Nat. Acad. Sci.*, **2000**, *97*, 14046.

[77] Harries, D.; May, S.; Ben-Shaul, A. *Colloids and Interfaces A*, **2002**, *208*, 41.

[78] May, S.; Harries, D.; Ben-Shaul, A. *Phys. Rev. Lett*, **2002**, *89*, 268102.

[79] Schiessel, H.; Aranda-Espinoza, H. *Eur. Phys. J. E*, **2001**, *5*, 499.

[80] Harries, D.; May, S.; Ben-Shaul, A. *J. Phys. Chem. B.*, **2003**, *107*, 3624.

[81] O'Hern, C. S.; Lubensky, T. C. *Phys. Rev. Lett.*, **1998**, *80*, 4345.

[82] O'Hern, C. S.; Lubensky, T. C.; J.Toner. *Phys. Rev. Lett.*, **1999**, *83*, 2745.

[83] Golubovic, L.; Golubovic, M. *Phys. Rev. Lett.*, **1998**, *80*, 4341.

[84] Rädler, J. O.; Koltover, I.; Jamieson, A.; Salditt, T.; Safinya, C. R. *Langmuir*, **1998**, *14*, 4272.

[85] Koltover, I.; Salditt, T.; Safinya, C. R. *Biophys. J.*, **1999**, *77*, 915.

[86] Bruinsma, R. *Eur. Phys. J. B*, **1998**, *4*, 75.